Received: 25 May 2022 | Revised: 14 November 2022 | Accepted: 23 November 2022

DOI: 10.1002/eqe.3791

RESEARCH ARTICLE

WILEY

Accounting for earthquake-induced ground-motion duration in building-portfolio loss assessment

Kenneth Otárola[1] | **Roberto Gentile**[2] | **Luis Sousa**[3] | **Carmine Galasso**[1,4]

[1]Department of Science, Technology and Society, Scuola Universitaria Superiore (IUSS) Pavia, Pavia, Italy

[2]Institute for Risk and Disaster Reduction, University College London, London, UK

[3]Research and Resilience, Verisk – Extreme Event Solutions, London, UK

[4]Department of Civil, Environmental, and Geomatic Engineering, University College London (UCL), London, UK

Correspondence
Carmine Galasso, Department of Civil, Environmental, and Geomatic Engineering, University College London (UCL), Gower St, WC1E 6BT, London, UK.
Email: c.galasso@ucl.ac.uk

Funding information
Italian Ministry of Education, University and Research at IUSS Pavia; UK Research and Innovation, Global Challenges Research Fund, Grant/Award Number: NE/S009000/1 at UCL

Abstract

Earthquake-induced ground-motion duration can have a non-negligible impact on the nonlinear seismic performance of structures. However, in current seismic risk assessment practice, hazard and vulnerability analyses generally only consider ground motion's amplitude and frequency-content features, often relegating duration to implicit considerations. This study introduces a simulation-based framework to explicitly quantify the impact of ground-motion duration on building-portfolio direct economic losses. Case-study synthetic building portfolios located at different distances from a case-study seismic source (i.e., fault) are assembled considering – individually and in combination – three building typologies representing distinct vulnerability classes in Southern Italy. Such typologies correspond to non-ductile moment-resisting reinforced concrete (RC) infilled frames designed to only sustain gravity loads (i.e., *pre-code* infilled frames), and ductile moment-resisting RC infilled and bare frames designed considering seismic provisions for high-ductility capacity (i.e., *special-code* infilled and bare frames). Event-based probabilistic seismic hazard analysis is performed explicitly simulating duration jointly with spectral-shape-related intensity measures (IMs), accounting for their spatial and cross-correlation. Sets of ground-motion records are selected to conduct cloud-based nonlinear time-history analyses (NLTHAs) and derive fragility models for each considered building typology through archetype structures, simulating their structural response using computational models that account for stiffness and strength cyclic and in-cycle deterioration as well as destabilising $P-\Delta$ effects. Fragility models are derived using average pseudo-spectral acceleration (in a range of periods of interest) as the primary IM and alternatively: (1) the dissipated hysteretic energy as an engineering demand parameter (EDP), implicitly accounting for duration given the cumulative nature of such an EDP and the adopted nonlinear modelling strategy, in a scalar format; (2) the dissipated hysteretic energy as an EDP, as before, explicitly considering duration as an IM together with spectral shape, in a vector-valued format. Vulnerability models are then derived using

the fragility models and appropriate building-level damage-to-loss models. The portfolio loss exceedance curves and expected annual losses computed for each combination of exposure, hazard, and vulnerability models are critically assessed and discussed. Depending on the portfolio's size, exposure composition, location relative to the fault, site conditions and the seismic source model, the impact of duration on the loss estimates can be significant. For the considered settings, relative variations up to 200% between the scalar- and vector-valued-based portfolios expected annual losses are observed, attaining the highest discrepancies as the fault-to-portfolio distance increases.

KEYWORDS
building-portfolio direct economic loss, dissipated hysteretic energy, earthquake-induced ground-motion duration, expected annual loss, loss exceedance curve, vector-valued fragility model

1 | INTRODUCTION

Major earthquake events worldwide have resulted in devastating human, economic and environmental losses in modern societies. Regional seismic risk assessment represents the first step for risk-informed decision-making on potential risk-mitigation strategies and resilience-enhancing policies for earthquake-prone regions. Generally, seismic risk assessment requires three main modelling components: (1) a seismic hazard model, which in its probabilistic format simulates representative earthquake scenarios in time and space and assesses the resulting ground-motion intensities across a geographical area at risk; (2) a comprehensive exposure dataset, containing details on the location and characteristics of the assets at risk in the geographic area of concern; (3) a set of vulnerability models for those exposed assets/asset types, quantifying the susceptibility to damage or other forms of loss (e.g., downtime and casualties) of structures and their contents because of the hazard impact (e.g., in ref. 1). The latter component plays a key role in seismic risk quantification/risk reduction since reducing physical vulnerability leads to a direct decrease in the associated risk. Hence, understanding, modelling, and quantifying the various earthquake-induced ground-motion characteristics driving seismic vulnerability becomes essential.

Current seismic risk assessment procedures characterise ground motions in terms of amplitude and frequency content (e.g., through a ground-motion response spectrum), usually without explicitly considering duration. However, large-magnitude earthquake events worldwide resulting in long-duration ground motions have emphasised the need to account for duration in more realistic/practical engineering applications (e.g., in ref. 2). The significance (and influence) of amplitude and frequency-content characteristics on ground-motion-induced damage/losses have already been comprehensively investigated and quantified (e.g., in refs. 1, 3). However, it is not until recent years that some consensus has been reached on the impact of duration on structural response (e.g., in refs. 4, 7), but not wholly on resulting ground-motion-induced damage/losses, given the limited investigation on this subject (e.g., in ref. 5). The conflicting findings from past literature (e.g., in ref. 6) mainly resulted from the adopted intensity measures (IMs) to define ground-motion duration, the engineering demand parameters (EDPs) utilised to quantify structural response, and the building computational models' inadequacy in capturing the stiffness and strength cyclic and in-cycle deterioration of the structural components and destabilising $P-\Delta$ effects (e.g., in ref. 7).

It has been discussed in the literature (e.g., in refs. 8, 9) that while ground-motion duration has no significant effect on peak-based EDPs (e.g., maximum inter-storey drift ratio, MIDR), it can significantly impact cumulative-based ones (e.g., dissipated hysteretic energy, E_H). However, noteworthy advances on the topic have been recently made due to the increasing availability of reliable long-duration ground-motion records and advanced building computational models able of appropriately capture damage accumulation (e.g., in refs. 4, 7). Those studies have demonstrated that duration-related effects are more apparent when structural components approximate their ultimate deformation and start to strain-soften, even when peak-based EDPs are employed, while those are marginally influenced by duration at lower deformations. Such recent literature has mainly investigated the influence of duration on structural collapse capacity and risk. Recent studies have also proposed novel ground-motion record selection procedures to decouple duration effects from the spectral shape

by using spectrally-equivalent long- and short-duration ground-motion records. It is worth noting that such an approach assumes a weak correlation between spectral-shape- and duration-related IMs, which may not be a realistic assumption in some scenarios, as demonstrated by Huang et al.[10], among others (e.g., in ref. 11). Such study showed that ground-motion spectral shape and duration are correlated for structures with fundamental structural periods under 1.5–2.0 s.

The main difficulty in quantifying duration impact on structural response and associated damage/losses is the challenging task of decoupling duration effects from those related to other ground-motion characteristics. Literature describing how duration influences structural fragility for different damage states (DSs) and the detailed quantification of such influence is not widely available (e.g., in refs. 12, 13); therefore, this modelling challenge was recently tackled using two different approaches in Otárola, Gentile, et al.[14] and Otárola, Sousa, et al.[15] In the first approach, the effect of duration was decoupled from the effects of ground-motion amplitude and spectral shape by assembling sets of spectrally equivalent long- and short-duration ground-motion records similarly to other authors (e.g., in ref. 16). Then, those sets of records were employed in comparative incremental dynamic analyses to derive fragility and vulnerability relationships using single-degree-of-freedom deteriorating nonlinear computational models. Based on statistical hypothesis testing on the obtained fragility estimates, it was observed that duration could significantly impact several DSs (i.e., others than collapse), especially when using cumulative-based EDPs and for highly-deteriorating structures. In the second approach, the generalised conditional intensity measure (GCIM) approach[17] was employed to select hazard-consistent ground-motion records (e.g., in refs. 2, 18). Those records were used as an input to cloud-based nonlinear time-history analyses (NLTHAs) using realistic multi-degree-of-freedom deteriorating building computational models. Duration impact was investigated through variance analysis, confirming that cumulative-based EDPs are better correlated to ground-motion duration; and in terms of fragility/vulnerability models conditioned on a vector-valued IM, jointly considering duration and spectral shape.

As discussed above, most of the existing research focused on structural response/structural performance assessments, with only a very few studies investigating building-specific loss assessments (e.g., ref. 5). To the Authors' knowledge, no past studies investigated the influence of duration on building-portfolio direct economic losses, accurately quantifying the potential impact of ground-motion duration and spectral shape on the loss estimates of building portfolios located in earthquake-prone regions, as proposed in this study. This can interest different stakeholders (e.g., government agencies, property owners, (re-)insurers, among others), who need to cope with the reduction/transfer of seismic risk using various strategies (e.g., seismic design legislation, seismic retrofit ordinances, earthquake insurance policies). Hence, based on the existing knowledge, the potential risk estimations for basing these decisions must be as dependable as possible, regardless of the chosen risk reduction or risk transfer mechanisms. This study intends to fill the previously discussed knowledge gap, investigating the impact of earthquake-induced ground-motion duration in conjunction with spectral shape on building-portfolio direct economic loss assessment for better risk-informed decision-making on potential risk-mitigation strategies and resilience-enhancing policies in earthquake-prone regions.

Specifically, this study implements a simulation-based seismic loss assessment framework. The proposed methodology relies on event-based probabilistic seismic hazard analysis (PSHA), cloud analysis-based (e.g., in ref. 19) vulnerability derivation (including models conditioned on scalar and vector-valued IMs; e.g., in ref. 20), and simulation-based loss estimation (e.g., in refs. 21, 22). The results obtained using a scalar IM are used as a benchmark case since these IMs are employed commonly in practice. The differences when using scalar or vector-valued IMs are of particular interest in this study to quantify the impact of utilising a vector-valued IM. The approach is applied to 12 case-study synthetic building portfolios of diverse sizes, located next to a case-study seismic source (i.e., fault). Different building typologies are considered for each portfolio (i.e., different exposures), including gravity- and/or seismically-designed moment-resisting reinforced concrete (RC) building frames in infilled and bare (this to account for modern buildings with masonry partitions not significantly contributing to global strength and stiffness but with a similar cost to actual contributing masonry infills) configurations. Results are discussed considering duration-related effects on the (median) loss exceedance curves and the expected annual loss (EAL) of the considered portfolios at different distances from the case-study fault. The main objective is to implement a simulation-based seismic loss assessment framework including ground-motion duration and spectral shape on both the hazard and fragility/vulnerability analysis; hence, improving the state-of-practice in catastrophe risk modelling (e.g., in ref. 23).

This paper is organised as follows. Section 2 describes the adopted simulation-based seismic loss assessment approach, including details concerning hazard analysis, fragility/vulnerability modelling, and loss assessment. Section 3 introduces an illustrative application of the proposed methodology, discussing the selected building typologies, the developed case-study synthetic portfolios and the assembled stochastic catalogue (i.e., a seismicity realisation over a defined period of

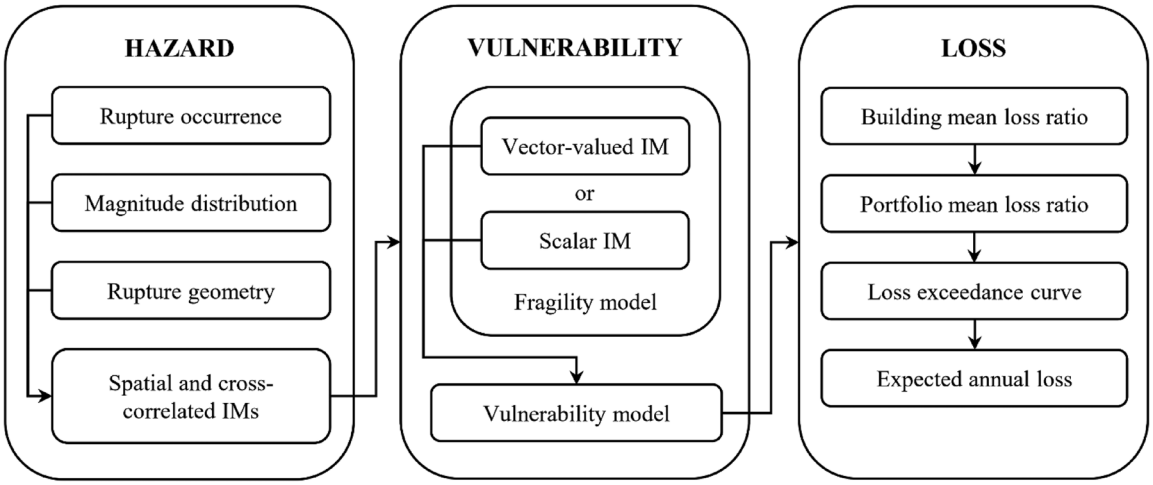

FIGURE 1 Adopted methodology for simulation-based seismic loss assessment of building portfolios jointly accounting for earthquake-induced ground-motion duration and spectral shape. IM, intensity measure

time). Section 4 presents the main findings from the analyses, which are discussed based on thoroughly examining the results. Section 5 outlines the main conclusions of this study.

2 | SIMULATION-BASED SEISMIC LOSS ASSESSMENT

The framework for simulation-based seismic loss assessment accounting for earthquake-induced ground-motion duration is illustrated in Figure 1. The framework's relevant probabilistic modules (i.e., hazard analysis, vulnerability modelling and loss assessment) are detailed in the following subsections. Case-study synthetic building portfolios are assembled to implement the proposed framework, considering different building typologies. Each building portfolio consists of several locations distributed in an equally-spaced grid according to its corresponding size. Based on the selected typology/typologies, a group of buildings is collocated per location (i.e., the exposure is "lumped").

The hazard module relies on event-based PSHA (e.g., in ref. 24) to simulate the seismicity in the considered region (as described by a source model) and the resulting ground-motion IMs (amplitude- and duration-related) at the considered locations as defined by a ground-motion model (GMM) and using appropriate cross- and spatial cross-correlation models. Specifically, a stochastic event set (i.e., stochastic catalogue), representing seismicity realisations for a given time span, is generated based on the minimum rate of exceedance of interest for a given IM (λ; commonly 1×10^{-4} year^{-1}). The number of earthquake occurrences within the stochastic catalogue is simulated by sampling the probability distribution for the considered source model's rupture occurrence. The geometry (constraining the earthquake rupture location) and the magnitude-frequency distribution (defining the mean annual occurrence rate over a magnitude range) describe the considered source model. For each location in the defined region, the resulting IM versus λ relationship (i.e., hazard curve) is derived (e.g., in ref. 25). The λ related to each IM value in the hazard curve is calculated by dividing the number of exceedances of that IM value by the length of the stochastic event set. It is worth noting that ground-motion IM realisations from hazard curves (associated with a mean return period, T_R, equal to λ^{-1}) at a set of locations form a ground-motion field (i.e., a map of the seismic hazard based on ground-motion IM realisations related to a λ value). Several ground-motion fields are generated in this study to adequately capture the aleatory variability (both between- and within-event) in the chosen GMM and correlation models.

The vulnerability module relies on cloud-based NLTHAs performed using ground-motion records selected through the GCIM approach. It is worth mentioning that the GCIM approach performs site-specific ground-motion record selection; nevertheless, the selected records are assumed to be representative of the region in analysis, given their seismological features and ground-motion characteristics. The amplitude-based conditioning IM chosen for this study is the average pseudo-spectral acceleration (SA) over a range of structural periods of interest ($avgSA$). Such an IM is more efficient and sufficient than other typical IMs (e.g., in refs. 26, 27), meaning, in turn, that fragility/vulnerability analysis results are less sensitive to other seismological features (such as magnitude and source-to-site distance) and characterised by

relatively low variability. Probabilistic seismic demand models (PSDMs) are developed using scalar and vector-valued IMs through linear regression. Fragility models for diverse damage states (DSs) are derived for each considered building typology (through appropriate archetype structures) within the case-study building portfolios. The mean loss ratio (LR) is then calculated using the developed fragility models and a building-specific damage-to-loss model for each location, building type and simulated IM through the total probability theorem.

The loss module computes building-portfolio loss exceedance curves (i.e., mean annual frequency of exceedance, MAFE, versus mean LR) using the simulated ground-motion fields, from where lists of events, and thus associated mean LRs are obtained (utilising the corresponding vulnerability models and the IMs at each location). These lists can be sorted from the highest mean LR to the lowest. The MAFE related to each mean LR value is calculated by dividing the number of exceedances of that mean LR value by the length of the stochastic event set (eventually multiplied by the number of stochastic event sets, if more than one set is generated). Assuming that the rupture occurrence model follows a Poisson process (i.e., the simulated earthquake events have exponentially distributed interarrival times), the probability of exceedance of each mean LR can also be estimated using the exponential cumulative distribution function. Finally, the building-portfolio EAL can be calculated by averaging the mean LRs across all the simulations and events.

2.1 | Hazard analysis

A stochastic event set is assembled following the assumption that the occurrence of events on a case-study strike-slip fault located in Southern Italy follows a Poisson recurrence model. The characteristic earthquake-recurrence model by Convertito et al.[28] is adopted to simulate the moment magnitude (M_w) of each earthquake event. The magnitude-dependent length of the rupture is obtained from the equations proposed by Wells and Coppersmith,[29] and the Joyner-Boore distance (R_{JB} – the shortest distance from a site to the surface projection of the rupture plane; in ref. 30) is used to define the source-to-site distances for the set of target locations. Time-independent rupture occurrence models like the one used here (i.e., homogeneous Poisson process-based model) do not adequately capture the time-dependency of earthquake events on specific fault segments since the probability of having a similar magnitude earthquake might be lower than average after a segment rupturing earthquake. To address this issue, time-dependent rupture occurrence models are becoming more popular (e.g., in ref. 31), particularly for fault-based PSHA (e.g., as in ref. 32), but their investigation is outside the scope of this study. The selected amplitude- and duration-related IMs for this study are $avgSA$ and 5%–95% significant duration (Ds_{5-95}), respectively. It is worth noting that $avgSA$ is estimated as the geometric mean of several SA ordinates, which are: 0.2 T_1; min[1.5 T_2, (T_1 + T_2)/2]; 1.0 T_1; 1.5 T_1; 2.0 T_1.[33] Thus, a total of six IMs are simulated during the event-based PSHA to finally obtain the two selected IMs (i.e., $avgSA$ and Ds_{5-95}). T_1 and T_2 are the first and second modal structural periods of a given structural archetype representative of a building typology, respectively.

The selected ground-motion amplitude- and duration-related IMs for each earthquake event in the stochastic event set are simulated using GMMs calibrated from Italian strong-motion records for amplitude- and integral-based IMs.[34,10] These GMMs describe the marginal probability distribution of ground-motion IMs at a specific location, given a rupture scenario and site conditions. Equation (1) shows the format of the GMM at location j due to earthquake event k. $ln(IM)_{k,j}$ is the natural logarithm of the IM of interest; $ln(\overline{IM})_{k,j}$ is the estimated mean of the natural logarithm of the IM of interest; τ_k is the between-event (i.e., inter-event) standard deviation; $\sigma_{k,j}$ is the within-event (i.e., intra-event) standard deviation; η_k is a standard Normal between-event (i.e., inter-event) residual due to an earthquake event k; and $\varepsilon_{k,j}$ is a standard Normal within-event (i.e., intra-event) residual for the location j due to an earthquake event k (e.g., in ref. 35). It is worth noting that the residuals have several essential characteristics, and studies (e.g., in ref. 36) have shown that: (1) the marginal between- and within-event residuals of an SA ordinate can be represented by a Normal distribution; (2) the between- and within-event residuals of SA ordinates at one location can be represented by a multivariate Normal distribution; (3) the within-event residuals at different locations can be represented by a bivariate Normal distribution. Some other studies (e.g., in ref. 17, 37) indicated that the marginal between- and within-event residuals of an arbitrary IM could also be represented by a Normal distribution, and the between- and within-event residuals between an arbitrary vector of IMs (e.g., Ds_{5-95}) can be also represented by a multivariate Normal distribution. Hence, it can be assumed that a multivariate Normal distribution can approximate the between- and within-event residuals across the selected IMs, and at multiple locations specifically for within-event residuals (e.g., in ref. 38). Note that such an assumption needs to be verified using densely distributed ground-motion data as specified in Du and Ning.[39] However, such verification is out of the scope of this study.

$$ln(IM)_{k,j} = ln\left(\overline{IM}\right)_{k,j} + \tau_k \eta_k + \sigma_{k,j}\varepsilon_{k,j} \quad (1)$$

For each earthquake event, k, the simulation procedure incorporates both spatial and cross-correlations for the residuals as appropriate. The η_k values exhibit cross-correlation between different IMs at the same location, which is constant across all the locations. The η_k values are simulated utilising the cross-correlation models developed by Huang and Galasso[34] (between SA ordinates) and Huang et al.[10] (between SA ordinates and Ds_{5-95}, with correlation coefficients varying between −0.6 to 0.1), following the suggestion of Goda and Hong[40] (i.e., approximating these residuals using empirical correlation models related to the total, rather than the specific between-event, GMM aleatory variability). To this end, the approach presented by Bradley[41] to obtain correlated random realisations of the residuals from a multivariate Normal distribution is adopted. The $\varepsilon_{k,j}$ values exhibit spatial and cross-correlation between different IMs at multiple locations (when considering more than one location), where locations close to each other are more likely to experience similar ground-motion intensities than locations farther apart. The $\varepsilon_{k,j}$ values are simulated using the spatial cross-correlation model developed by Du and Ning[39] (between SA ordinates; between SA ordinates and Ds_{5-95}). To this end, the approach presented by Markhvida et al.[38] based on Principal Component Analysis and geostatistics to obtain spatial cross-correlated random realisations of the residuals is adopted (similar to the outcomes obtained using the model developed in Loth and Baker[35]), significantly reducing the computational burden. Several simulations are performed for each earthquake event in the stochastic catalogue to capture the between- and within-event aleatory variability in the selected GMM; the number of simulations is based on a sensitivity analysis developed by the authors to obtain stable (i.e., stationary) results regarding the computed median hazard curves. It is worth noting that different GMMs should be considered and combined in a logic tree to consider the epistemic uncertainties included in the framework. Nevertheless, only one model for each IM is utilised here since this study is intended to introduce the proposed simulation-based seismic loss assessment framework and performs a comparative (i.e., relative) analysis rather than providing absolute results.

2.2 | Vulnerability modelling

Vector-valued IMs use two or more ground-motion parameters to estimate a structure's response with higher efficiency than scalar IMs, and attain sufficiency when scalar IMs do not guarantee it.[42] Fragility models are herein derived using cloud-based NLTHAs using $avgSA$ as the primary IM and alternatively, for relative comparison: (1) E_H as the EDP, implicitly accounting for duration given the cumulative nature of such EDP and through the adopted nonlinear modelling strategy, in a scalar format; (2) E_H as the EDP as before, and explicitly considering duration as an IM together with spectral shape, in a vector-valued format. It is considered that a PSDM conditioned on a vector-valued IM increase the fragility/vulnerability estimates' reliability compared to one conditioned on a scalar IM, as it is commonly implemented. It is worth noting that to simulate the structural response, the building computation models considered in this study account for the destabilising $P-\Delta$ effects and stiffness and strength cyclic and in-cycle deterioration of structural components[43,44] relying on E_H – following the deterioration rule developed by Rahnama and Krawinkler.[45] This allows capturing the cumulative damage due to increasing ground-motion duration (e.g., in ref. 14, 15). Vulnerability models are then derived by combining the above fragility models with a building-specific damage-to-loss model. When using a scalar IM (i.e., $avgSA$), the probability of reaching or exceeding a DS at a given IM level can be estimated as proposed by Jalayer and Cornell[19] using linear regression through the ordinary least squares approach to develop a scalar-based PSDM following a power-law functional relationship between the considered IM and EDP. Instead, when using a vector-valued IM (i.e., $[avgSA, Ds_{5-95}]$), the probability of reaching or exceeding a DS at given IM levels can be estimated as proposed by Otárola, Sousa, et al.[15] using multiple linear regression through the ordinary least squares approach to develop a vector-valued-based PSDM (collinearity between IMs is dismissed through collinearity diagnostic; e.g., in ref. 46). Equation (2) provides the probability of reaching or exceeding a given DS. In such equation, $\mu_{EDP|\boldsymbol{IM}}$ and $\sigma_{ln(EDP)|ln(\boldsymbol{IM})}$ are the linear median and logarithmic standard deviation of the structural response given no collapse (as obtained from the PSDMs), $\boldsymbol{IM}$ represents a scalar or vector-valued IM as appropriate, and e_{h,ds_i} corresponds to the i^{th} DS threshold expressed in E_H (i.e., energy) terms.

$$P(E_H \geq e_{h,ds_i}|\boldsymbol{IM}, NC) = 1-\Phi\left[\frac{ln\left(e_{h,ds_i}\right)-ln\left(\mu_{EDP|\boldsymbol{IM}}\right)}{\sigma_{ln(EDP)|ln(\boldsymbol{IM})}}\right] \quad (2)$$

Energy-based DS thresholds are defined using the stable relationship between MIDR and E_H[47] allowing retaining the confidence of widely accepted and experimentally-calibrated deformation-based DS thresholds, as in Equation (3) and detailed in Otárola, Sousa, et al.[15] Such equation is fitted in median terms using least-squares nonlinear regression in

the log-log space, where a_0, a_1, a_2, and a_3 are the coefficients of the regression. E_H is selected as an EDP because it is a cumulative measure that monotonically increases with the length of the applied excitation, unlike MIDR. Thus, E_H enables the development of statistical models consistent with the physics of a structure subjected to long-duration ground motions (e.g., in ref. 48), accounting for the severity and number of inelastic cycles the structure may undergo. In other words, using E_H enables better capturing the whole range of structural behaviour from structural yielding up to collapse. Most prior studies derive seismic fragility in terms of MIDR thresholds, although in some cases, this is considered in conjunction with the residual inter-storey drift. To the best of the Authors' knowledge, no energy-based DS thresholds are readily available in the literature. Arguably, it is challenging to estimate the global structural capacity in terms of E_H to define reliable DS thresholds, which are more easily (and widely) defined based on using peak deformation parameters (e.g., MIDR). In this study, the ground-motion MIDR versus E_H pairs are used to calibrate the median E_H versus MIDR relationship and converting the MIDR-based DS thresholds into E_H-based ones, thus allowing us defining E_H-based fragility relationships. Consistently with the common practice of neglecting the variability of the MIDR thresholds in performing MIDR-based fragility relationships, the MIDR to E_H conversion is herein carried out neglecting the $E_H|$MIDR variability. The existence of a stable relationship between a peak deformation parameter and E_H (e.g., MIDR versus E_H) has been confirmed by numerical dynamic analyses of SDoF systems subjected to ground motions (e.g., in refs. 48, 49) and quasi-static, cyclic experimental tests on individual structural components (e.g., in refs. 50, 51). A wide distribution of Ds_{5-95} is used to build such relationship, avoiding bias in the estimations due to an improper consideration of the structural response variability due to ground-motion duration. It is observed that duration is well correlated to the amount of hysteretic energy dissipated by a structure[47]; therefore, duration can explain the variability of E_H given MIDR, because Ds_{5-95} can be a good proxy for the number of plastic excursions of a system. Nevertheless, relevant experimental/field data may be used to provide a deeper confirmation to such hypothesis. It is worth mentioning that structural response representing (fully) elastic cases (i.e., near-zero E_H values) and collapse cases are omitted in the regression analysis when deriving the energy-based DS thresholds.

$$E_h\ (MIDR) = \exp\left(a_0 MIDR^{a_1} + a_2 MIDR^{a_3}\right) \tag{3}$$

Logistic regression (for single or multiple IMs)[52] is used to estimate the probability of collapse conditioned on $\boldsymbol{IM}$ as shown in Equation (4). In this equation d_0 and d_i are the coefficients to be estimated from this regression (d_i indicates additional coefficients utilised in the regression, while IM_i indicates additional IMs utilised in the regression, both depending on the size n of $\boldsymbol{IM}$). In this study, structural collapse (dynamic instability not associated with a numerical value of the EDPs) is defined as reaching a MIDR of 4.00% for the PI frame and 8.00% for SI and SB frames. Such collapse DS thresholds are indifferently used when using MIDR or E_h (as in this study) as an EDP to produce the collapse fragility models. If a single structural response (i.e., record) causes a collapse, a value equal to one is assigned and zero otherwise, in the logistic regression. The collapse and non-collapse cases are then combined using the total probability theorem as shown in Equation (5), which is used to compute the conditional probability of exceeding a DS conditioned on $\boldsymbol{IM}$ (e.g., in ref. 42). NC stands for non-collapse, and C stands for collapse in the specified equations as appropriate. It is worth mentioning that the building-specific DSs are calibrated via pushover analyses considering multiple measurable criteria (Table 1[53]) and defined later for each building typology in MIDR terms – and subsequently in E_H terms as explained above.

$$P\ (C|\boldsymbol{IM}) = \frac{1}{1 + e^{-\left[d_0 + \sum_{i=1}^{n} d_i ln(IM_i)\right]}} \tag{4}$$

$$P(E_H \geq e_{h,ds_i}|\boldsymbol{IM}) = P\,(C|\boldsymbol{IM}) + [1 - P\,(C|\boldsymbol{IM})]\,P(E_H \geq e_{h,ds_i}|\boldsymbol{IM}, NC) \tag{5}$$

Damage-to-loss ratios (DLRs) are frequently empirically estimated through post-earthquake reconnaissance or expert judgment. Since this study involves mid-rise RC-infilled Italian buildings, a modified version of the DLRs suggested by Di Pasquale et al.[54] is used (i.e., adopting four DSs rather than five, by just averaging the associated DS3 and DS4). The defined DLRs for this study are: (1) 0.01 for slight damage (DS1); (2) 0.10 for moderate damage (DS2); (3) 0.55 for extensive damage (DS3); (4) 1.00 for complete damage (DS4). DS1 does not apply to the SB frame since this DS is associated with the first cracking of the masonry infills. The vulnerability models are expressed in terms of mean LR; in other words, in terms of the repair-to-replacement cost ratio of the building, conditional on $\boldsymbol{IM}$ as defined earlier. According to Equations (6) and (7), such models are derived using the total probability theorem. DLR_i is the expected damage-to-loss ratio for the i^{th}

TABLE 1 Criteria used to define the MIDR-based DS thresholds of the case-study frames

Damage level	Slight damage (DS1)	Moderate damage (DS2)	Extensive damage (DS3)	Complete damage (DS4)
Section level	N/A	Reaching yield bending strength in a supporting column.	Reaching maximum bending strength at any column.	Reaching shear failure in any of the components.
Component level	First masonry infill panel starts to develop cracks.	Reaching yield rotation in a supporting column.	Reaching 75% ultimate rotation in any component.	Reaching ultimate rotation in any component.
Global level	N/A	Reaching global yield strength of the structure.	Reaching global maximum strength of the structure.	Reaching 20% drop in global maximum strength of the structure.
DSs description	Non-structural damage only due to masonry infill cracking.	Moderate structural and non-structural damage with no significant yielding of structural components.	Severe structural and non-structural damage. Some residual strength and stiffness are retained.	Full exploitation of strength and ductility. Very low residual strength and stiffness in the components.

DS (i.e., the level of damage), while $P(DS = ds_i | \boldsymbol{IM})$ is the probability that the DS is equal to ds_i (i.e., the probability of being in a DS) given $\boldsymbol{IM}$; noting that $P(DS = ds_4 | \boldsymbol{IM})$ equals $P(DS \geq ds_4 | \boldsymbol{IM})$. The DLR related to each DS is assumed to be the same for both the bare and infilled frames. Although the infills are not explicitly considered in the nonlinear model for the SB frame, consistently with common assumptions in practice, they undoubtedly contribute to losses (i.e., the partitions of the SB frame have a similar cost to the masonry infills). It is worth mentioning that the uncertainty of the DLRs (e.g., in refs. 55, 56) may strongly affect the loss estimation, particularly in terms of its variability.[57] Since relative (duration-dependent) loss estimates are of interest in this study (and the same DLRs are selected for each case-study frame) rather than absolute estimates, such uncertainty is neglected for simplicity. This is not expected to jeopardise the generality of the results. The uncertainty associated with the DLRs can generally influence median loss curves but not EAL estimations, an outcome of this study.

$$LR\ (\boldsymbol{IM}) = \sum_{i=1}^{4} DLR_i P(DS = ds_i | \boldsymbol{IM}) \tag{6}$$

$$P\ (DS = ds_i\ | \boldsymbol{IM}) = P(DS \geq ds_i | \boldsymbol{IM}) - P(DS \geq ds_{i+1} | \boldsymbol{IM}) \tag{7}$$

2.3 | Loss assessment

The mean LR is estimated using the corresponding vulnerability models for each event and associated $\boldsymbol{IM}$ simulations (i.e., ground-motion fields). This process is repeated at each location within the building portfolio, and for each considered building typology, t. According to Gentile and Galasso,[22] for each computed mean LR, the ground-up loss at each of the n_{loc} locations can be calculated through Equation (8), assuming $N_{b,t}$ buildings of typology t for which the replacement cost is equal to $CR_{b,t}$. Such cost (cost of structural/non-structural components and contents) is often provided in the exposure model. Hence, the mean LR for every location for a given $\boldsymbol{IM}$ is calculated with Equation (9). CR_{loc} is the total replacement cost of a location.

$$L_{loc}\ (\boldsymbol{IM}) = \sum_{t} LR_{b,t}\ (\boldsymbol{IM})\, N_{b,t} CR_{b,t} \tag{8}$$

$$LR_{loc}\ (\boldsymbol{IM}) = \frac{L_{loc}\ (\boldsymbol{IM})}{CR_{loc}} = \frac{\sum_t LR_{b,t}\ (\boldsymbol{IM})\, N_{b,t} CR_{b,t}}{\sum_t N_{b,t} CR_{b,t}} \tag{9}$$

Assuming for simplicity that $CR_{b,t} = CR$ for each building in a specific location, Equation (9) is simplified into Equation (10), in which $n_{b,t} = N_{b,t} / \sum_t N_{b,t}$ is the proportion of buildings of typology t. If the distribution of buildings n_b is

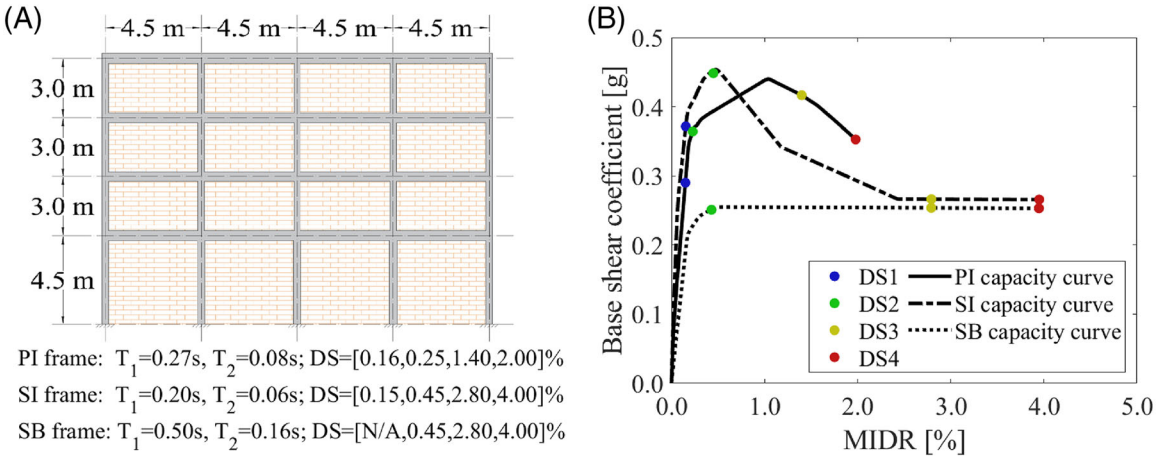

FIGURE 2 (A) Elevation layout and modal structural periods of the considered building typologies; (B) pushover capacity curves and DS thresholds definition (in MIDR terms) of the considered building typologies

considered uniform through the entire portfolio, the LR is calculated as the average of the LRs per location (Equation 11). Given such assumptions, there is no need to assume any *CR* nor the number of buildings at the given location for each building typology without losing generality of the results. The outcome is expressed in terms of (median) portfolio loss exceedance curves (or simply loss curves) and EAL, representing the expected loss per year (statistical mean loss). The EAL is calculated by averaging the portfolio mean LR for each event and $\boldsymbol{IM}$ in the stochastic event set.

$$LR_{loc}\ (\boldsymbol{IM}) = \frac{\sum_t LR_{b,t}\,(\boldsymbol{IM})\,N_{b,t}}{\sum_t N_{b,t}} = \sum_t LR_{b,t}\,(\boldsymbol{IM})\,n_{b,t} \tag{10}$$

$$LR_{loc}\ (\boldsymbol{IM}) = \frac{\sum_{loc} L_{loc}}{CR_{port}} = \frac{\sum_{loc} LR_{loc} CR_{loc}}{\sum_{loc} CR_{loc}} = \frac{\sum_{loc} LR_{loc}}{n_{loc}} \tag{11}$$

3 | ILLUSTRATIVE APPLICATION

3.1 | Considered building typologies

The case-study synthetic building portfolios are assembled considering – individually and in combination – three building typologies representing distinct vulnerability classes in Southern Italy. Such typologies correspond to: non-ductile moment-resisting RC infilled frames, designed to only sustain gravity loads (i.e., *pre-code* infilled frames; PI); ductile moment-resisting RC infilled and bare (to account for modern buildings with masonry infills not significantly contributing to global strength and stiffness; i.e., non-collaborating infills) frames, designed considering seismic provisions for high-ductility capacity (i.e., *special-code* infilled and bare frames; SI and SB, respectively). The building frames share the same geometry,[58] with a total height equal to 13.50 m, a first storey height equal to 4.50 m and upper storeys of 3.00 m, and bay spans of 4.50 m (Figure 2A; modal structural periods and DS thresholds are also presented for clarity). The *special-code* frames are designed and detailed according to the Eurocode 8 Part 3 (EC8-3) seismic provisions for high ductility class (EN 1998–3[59]). These provisions include capacity design, various requirements in terms of cross-sectional dimensions, and seismic detailing to ensure ductile global performance and prevent the formation of localised brittle failure mechanisms. The *pre-code* frame is designed for gravity loads only as per the Royal Decree n. 2239 of 1939 (Consiglio dei Ministri[60]) that regulated the structural design in Italy until 1974. Thus, the frame does not conform to modern seismic requirements and is characterised by a non-ductile behaviour due to the lack of capacity design principles, poor confinement, and susceptibility to developing brittle failure mechanisms (e.g., shear failures) – more details can be found in Aljawhari et al.[53]

The reinforced concrete's mean mechanical properties, such as the concrete's compressive strength and the steel rebar yield strength, represent those adopted in Italy. Specifically, the mean mechanical properties of the concrete are obtained

TABLE 2 Properties of the reinforced concrete

Parameter	Symbol	Units	PI frame	SI/SB frame
Compressive strength of the concrete	f_{cm}	MPa	19.00	37.00
Modulus of elasticity of the concrete	E_c	GPa	26.67	32.60
Yield strength of the steel rebar	f_{ym}	MPa	360.00	490.00
Modulus of elasticity of the steel rebar	E_s	GPa	200.00	200.00

TABLE 3 Properties of the masonry infills

Parameter	Symbol	Units	PI frame	SI frame
Compressive strength	σ_{m0}	MPa	2.20	4.20
Shear strength	τ_{m0}	MPa	0.44	0.33
Vertical gravity stress	σ_0	MPa	0.00	0.00
Sliding resistance	τ_0	MPa	0.39	0.23
Modulus of elasticity	E_m	GPa	2.40	2.31
Thickness of infills	t_m	cm	14.50	10.00

from Verderame et al.[86] investigations for the PI frame while being based on building construction current practice for the SI and SB frames, as indicated in Aljawhari et al.[53] The mean mechanical properties of the masonry infills are obtained from the investigations of Liberatore and Mollaioli[61] for the PI frame, while are obtained from the investigations of Mohammad Noh et al.[62] for the SI frame. The described material properties are summarised in Tables 2 and 3 for the RC and the masonry infills, respectively. It is worth noting that the SB frame is assumed to present very weak masonry infills functioning as partitions, those have been increasingly used, and they are more recommended to ensure better seismic performance since they minimize the effects of frame-infill interaction of the structural components.[63] Two-dimensional computational models are developed for each building frame. In the assumption that the buildings are regular and symmetric, the proposed models can simulate the structural response of the buildings in both horizontal directions equivalently under a ground motion (e.g., in ref. 64). A complete description of the numerical modelling strategy adopted can be found in the appendix of this study. Figure 2B shows the frames' capacity curves and the corresponding DS threshold definition (Table 1) for each case-study frame.

3.2 | Considered ground-motions

The seed ground-motion records to derive the fragility and vulnerability models are those used in Otárola, Sousa, et al.,[15] representative of typical ground motions in Southern Italy based on their seismological features and ground-motion characteristics. Such a ground-motion record set was initially assembled using the GCIM approach, a site-specific, hazard-consistent ground-motion record selection procedure. Since $avgSA$ and Ds_{5-95} are selected to represent the ground shaking intensity in this study, if the seed ground motions cover a wide range of such IMs, those records can be considered to perform fragility and vulnerability analysis of the case-study frames in regional (multi-site) engineering applications. Figure 3 shows the $avgSA$ versus Ds_{5-95} distribution of the seed ground-motion records for the PI frame. Indeed, such a distribution covers a wide range of those IMs needed to reliably describe the nonlinear structural response (such wide distribution of IMs is consistent among the study cases). Additionally, $avgSA$ has demonstrated being more efficient and sufficient than other typical IMs, meaning that fragility and vulnerability analysis outcomes are going to be less sensitive to seismological features and ground-motion characteristics.[65] It is worth mentioning that Zhong et al.[66] recently developed a method called the site-specific adjustment framework for incremental dynamic analysis. Such an approach offers significant efficiencies and convenience in evaluating structural response. It can be employed either to evaluate a specific structure at a specific location or, more broadly, to develop surrogate structural models that can be evaluated for hazard conditions at multiple locations in regional earthquake scenario studies.

To obtain the seed ground-motion records using the GCIM approach, the considered target site was Ponticelli – Napoli, Italy (latitude: 40.8516°, longitude: 14.3446°). This site is located over class C soil, according to EC8-3, with a mean shear wave velocity in the first 30 m of 331 m/s.[67] The considered vector of IMs included: Ds_{5-95}, peak-ground acceleration, and

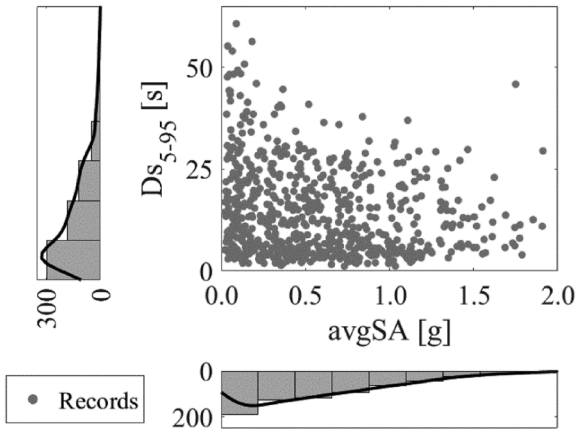

FIGURE 3 Selected seed ground-motion records for the PI frame: $avgSA$ versus Ds_{5-95} distribution and marginal $avgSA$ and Ds_{5-95} histograms with kernel smoothing function fit

35 SA ordinates (with structural periods from 0.10 to 4.00 s). A total of 17 sets of ground-motion records were selected for various conditioning intensity levels (i.e., SA at the fundamental structural period) between 0.05 and 2.00 g. The algorithm used for the ground-motion record selection is that proposed in Bradley,[41] where random realisations (i.e., simulations) of the selected IMs (consistent with the defined GCIM target distributions) are generated. Therefore, for each realisation of a vector of IMs, a ground-motion record with an identical IM vector can be ideally selected. In this study, the algorithm is slightly modified to admit a maximum amplitude scale factor of 5.00[68] and avoid repeated utilisation of the same seed ground-motion records within each specific conditioning intensity level. The selection is repeated for each case-study frame and each conditioning intensity level. The 40 ground-motion records within the database with the minimum misfit compared to the target distributions are selected per level (i.e., 680 records in total). This is done using the Kolmogorov-Smirnov goodness-of-fit testing. More related details on the ground-motion record selection procedure can be found in Bradley.[41] The ground-motion records are obtained from the Pacific Earthquake Engineering Research Centre – Next Generation Attenuation Relationships for Western United States database (NGA-West2[69]) dominated by shallow-crustal earthquake events, without considering pulse-like ground-motion records.

3.3 | Considered building portfolios

A total of 12 case-study synthetic building portfolios are considered in this study to investigate ground-motion duration impact based on their position, composition and size. A "region" normal to the longitudinal direction of the fault is first defined to perform the simulation-based loss assessment for such portfolios, with a size of 36 km × 115 km. Several locations are specified within the region, distributed on a uniform grid approximately 3 km-spaced according to Gentile and Galasso[22] (Figure 4A); hence, a 9 km^2 area pertains to each location (allowing a balance between computational burden and accuracy in the outcomes). The region is defined so that the closest locations are situated at 10 km minimum from the fault (to avoid directivity effects, at least conceptually). Just the locations within a specified portfolio (translucid areas in Figure 4A,B) are accounted for in the loss assessment context. Based on the selected building typologies, a group of buildings is collocated per location (i.e., the exposure is "lumped" at each location, as stated before).

Three different portfolio sizes are considered, assumed to represent diverse urban settings (e.g., a region, a metropolitan area, a city) defined as: (1) a base portfolio with 36 km × 36 km area (i.e., large portfolio); (2) a portfolio with 18 km × 18 km area (1/4 of base portfolio area; i.e., medium portfolio); (3) a portfolio with 9 km × 9 km area (1/16 of base portfolio area; i.e., small portfolio). Furthermore, four different exposure configurations are also considered, assuming each location has the same building composition. The first three configurations involve a single building typology (i.e., PI, SI or SB), and the fourth case represents a mixed composition; defined as: (1) 100%PI; (2) 100%SI; (3) 100%SB; (4) 60%PI + 32%SI + 8%SB (Italian typical building composition adopted from Gentile & Galasso[22]). Finally, the 12 stated synthetic portfolios are assembled considering all the composition and size combinations.

Given the proposed arrangements, the various portfolios are moved perpendicularly away from the fault within the specified region at 3 km intervals using their left boundary as reference. The aim is to evaluate ground-motion duration

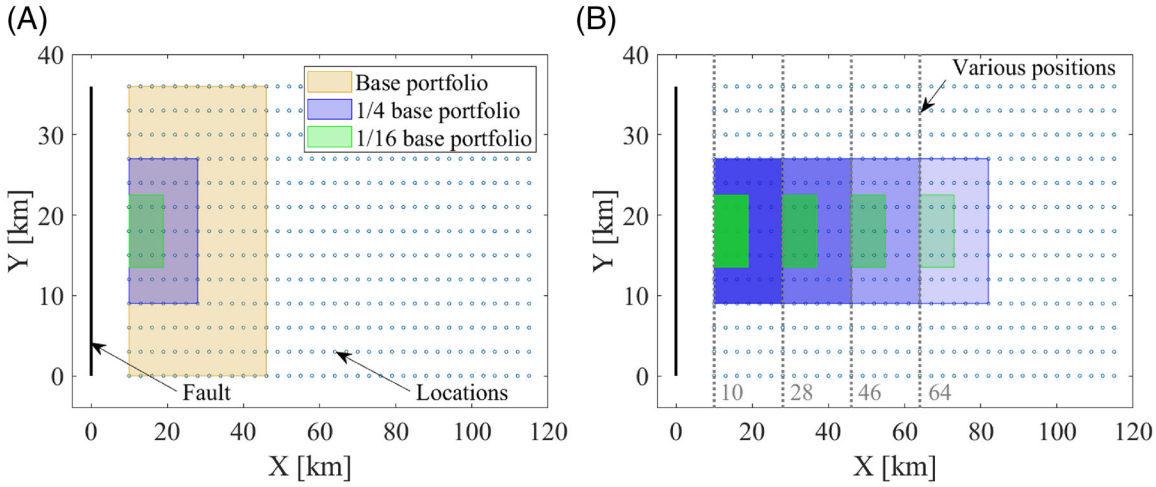

FIGURE 4 (A) Case-study building portfolios geometrical features and region definition; (B) Medium and small building portfolios located at various distances from the fault (i.e., 10, 28, 46 and 64 km). X and Y are the cartesian coordinates of the considered synthetic region

influence on the portfolios' direct economic losses as the distance from the fault varies. Duration's impact on the EAL estimates is studied at each position (i.e., every 3 km away from the fault up to 79 km). In contrast, the impact on the (median) loss exceedance curves is studied at specific distances for brevity (i.e., at 10, 28, 46 and 64 km from the fault; Figure 4B).

3.4 | Considerations for the stochastic catalogue

The considered fault rupture source model is defined by the characteristic earthquake-recurrence model introduced by Convertito et al.,[28] as cited before. Therefore, the necessary parameters for this model are arbitrarily assumed as follows: $m_c = 6.5$ (characteristic earthquake moment magnitude); $M_{w,min} = 5.0$ (minimum moment magnitude); $M_{w,max} = 7.0$ (maximum moment magnitude); $b = 1.0$ (b-value of the Gutenberg–Richter law); $\Delta m_1 = 0$ (interval below the magnitude level m_c, needed in the considered probabilistic model). The selected values are associated with a synthetic fault-rupture scenario developed in Gentile and Galasso,[22] following the recommendations by Convertito et al.[28] The annual rate of earthquake occurrence above a minimum threshold magnitude (i.e., $\nu(M_{w,min})$) equals 0.05. Using this value, the number of stochastic earthquake events and their interarrival times can be simulated up to a fixed time horizon associated with the desired catalogue length. Specifically, based on the proprieties of the Poisson model, such intervals are considered independent and follow an exponential distribution. The inverse transform sampling technique is used to develop a seismicity realisation using the exponential cumulative distribution function (the occurrence time to the first earthquake event is taken as a uniform time between 0 and 1 year). A 10,000-year (i.e., catalogue length) stochastic event set is considered, and 1,000 realisations of the two considered IMs are generated for each earthquake event within the stochastic catalogue. This catalogue length and number of realisations are selected based on the current catastrophe risk modelling practice and correspond to a good balance in terms of statistical validity of the loss estimates and computational burden based on a sensitivity analysis developed by the authors on median hazard curves (e.g., in ref. 71).

4 | RESULTS AND DISCUSSION

4.1 | Effects of ground-motion duration on hazard

Ground-motion duration increases with the distance from the source due to the scattering and dispersion of seismic waves and the difference in the arrival times of waves propagating at different velocities and traversing different paths (e.g., in refs. 72–74). However, duration also depends on local site conditions, with long-duration ground motions typically observed at sites with soft soils due to repeated seismic wave reflections within the softer layers.[75] Figure 5A and B show the obtained

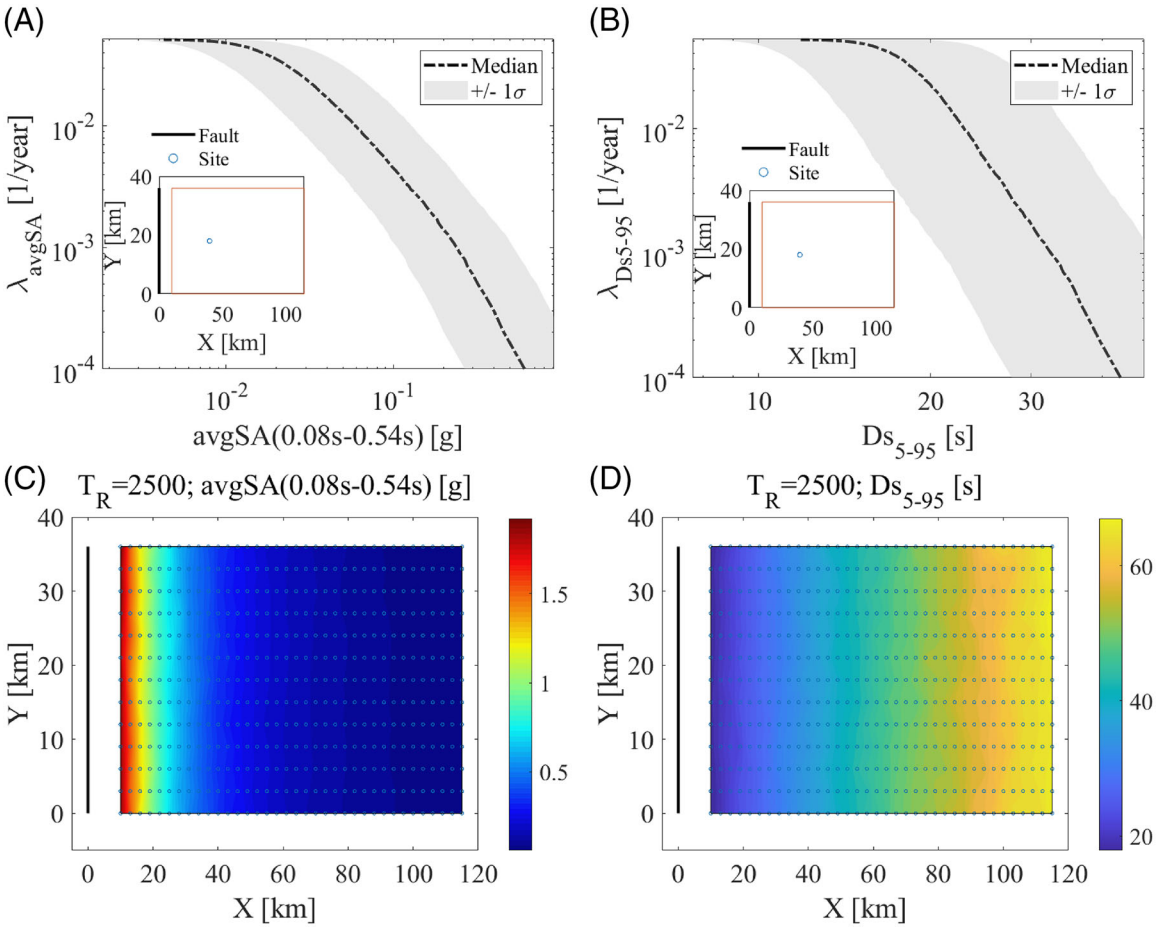

FIGURE 5 Event-based PSHA results for the PI frame: (A) $avgSA$ hazard curve for the indicated location; (B) Ds_{5-95} hazard curve for the indicated location; (C) 2500-year T_R (median) $avgSA$ ground-motion field; (D) 2500-year T_R (median) Ds_{5-95} ground-motion field

$avgSA$ and Ds_{5-95} hazard curves (median +/− a standard deviation; i.e., +/− 1σ) for the PI frame, respectively (λ is the mean annual frequency of exceedance $avgSA$, Ds_{5-95} or both jointly, as indicated using the corresponding subindex). Figure 5C and D show the (median) $avgSA$ and Ds_{5-95} ground-motion fields considering a 2500-year T_R (i.e., considering a λ equals 4×10^{-4} year^{-1}) earthquake event in the stochastic event set for the PI frame also, respectively. To better represent the joint variation of the correlated IMs, the marginal (median) hazard curves can be expressed as a single joint (median) hazard surface, as shown in Figure 6A for the exact location displayed in Figure 5A and B. According to the standard practice in event-based PSHA (e.g., in ref. 24), this surface can be simply derived by counting the number of realisations contemporarily exceeding an IM threshold pair ($avgSA$,Ds_{5-95}), divided by the total number of IM realisations. To transform such estimate of probability into an estimate of frequency, the result should be multiplied by $\nu(M_{w,min})$; as shown in Equation (12). In such an equation $avgSA$ and Ds_{5-95} are the IM thresholds of interest; $avgsa_{i,j}$ and $ds_{5-95i,j}$ are the IM realisations (associated with one event realisation, i out of e total events, and one GMM realisation, j out of r total realisations); and $I(avgSA \leq avgsa_{i,j}, Ds_{5-95} \leq ds_{5-95i,j})$ is an indicator function corresponding to 1 if an IM realisation pair (jointly) exceeds the defined IM thresholds and 0 otherwise. It is worth noting that several IM thresholds need to be investigated to construct such a joint hazard curve.

$$\lambda_{avgSA,Ds5-95} = \frac{\nu\left(M_{w,\min}\right)}{e \cdot r} \sum_{i=1}^{e} \sum_{j=1}^{r} I\left(avgSA < avgsa_{i,j}, Ds_{5-95} < ds_{5-95_{i,j}}\right) \tag{12}$$

As expected, the $avgSA$ values decrease with R_{JB} (i.e., $avgSA$ is negatively correlated with R_{JB}), while the opposite happens for Ds_{5-95} (i.e., Ds_{5-95} is positively correlated with R_{JB}); both IMs increase with M_w (i.e., $avgSA$ and Ds_{5-95} are positively correlated with M_w) (Figure 6B). No significant variability is noted between the considered IMs for the various locations at the same distance from the fault, given the simple adopted rupture occurrence model (i.e., a single strike-slip

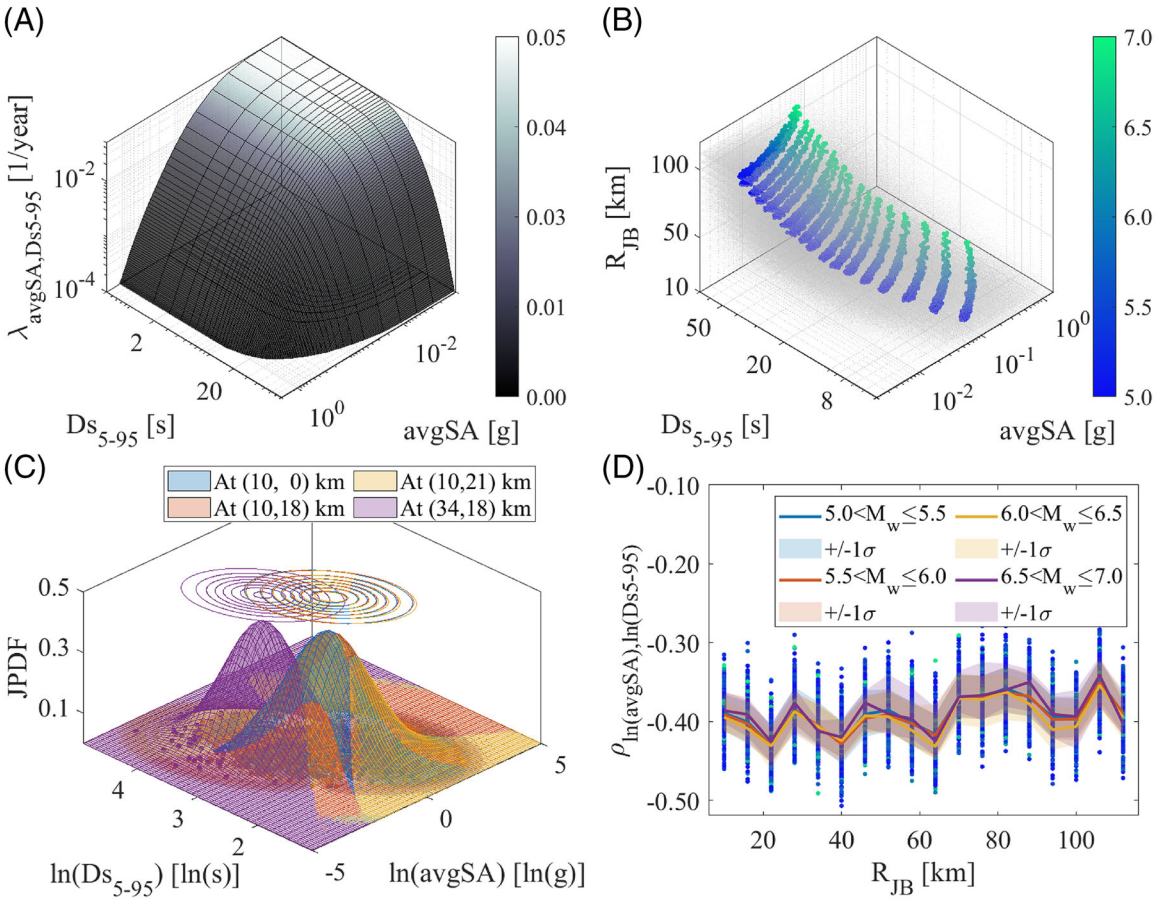

FIGURE 6 For the PI frame: (A) joint (median) hazard curve at the indicated location in Figure 5A and B; (B) scatter (grey cloud) and median (coloured cloud) $avgSA$ and Ds_{5-95} realisations at various locations aligned with the centre of the fault; (C) JPDF of the $avgSA$ and Ds_{5-95} realisations at the indicated locations according to Figure 4A and B; (D) variation of the $\rho_{ln(avgSA),ln(Ds5-95)}$ as a function of R_{JB} and M_w bins at various locations aligned with the centre of the fault. The colour bar in Figure 6B associated with the colour dots in Figure 6B and D indicates M_w

fault) and the considered source-to-site distance definition used for the GMMs. The $avgSA$ ground-motion field varies depending on the considered structural type (only one structural type is shown for brevity) since a different $avgSA$ definition is used for each case-study frame based on the geometric mean of the SA ordinates indicated earlier (since losses are simply added, having a different $avgSA$ definition for each frame is not considered a drawback). In contrast, the Ds_{5-95} ground-motion field is the same for every structural type. In the PI frame case, $avgSA$ ranges from approximately 0.05 up to 1.85 g; while the Ds_{5-95} ranges from approximately 18 up to 65 s within the defined rectangular region. This confirms that the seed ground-motion records utilised in deriving fragility and vulnerability models are appropriate for the loss assessment application developed in this study. It is worth mentioning that the joint distribution of $avgSA$ and Ds_{5-95} is bivariate lognormal (verified using the Henze-Zirkler's multivariate normality test in log-log space[76,36]), as illustrated by the joint probability density functions (JPDFs) in Figure 6C for the several considered locations, following the modelling assumptions described above. It can be noted that for distinct distances from the source, the $avgSA$ and Ds_{5-95} joint distributions remain particularly similar (i.e., mean and covariance almost identical) exhibiting a negative correlation, such correlation seems to be insensitive to both magnitude and distance (i.e., no systematic trends were found) as illustrated in Figure 6D and already observed by Baker and Bradley[77] and Huang et al.[10] for SA ordinates and Ds_{5-95}, for instance.

4.2 | Effects of ground-motion duration on vulnerability

Figure 7A and B show the fragility and vulnerability relationships obtained using $avgSA$ as an IM after performing cloud analysis, specifically for the SB frame. These relationships implicitly account for the Ds_{5-95} since the structure

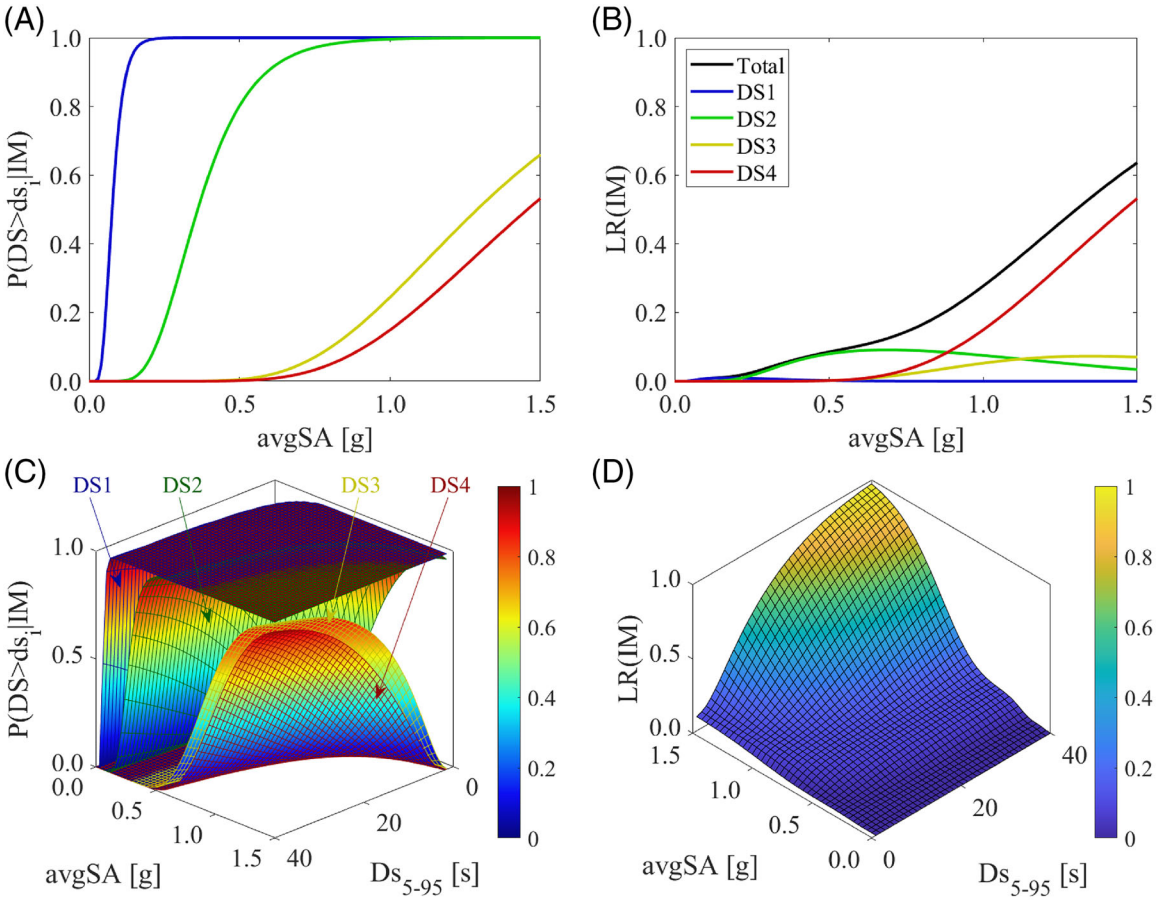

FIGURE 7 SB frame: (A) fragility relationships using a scalar IM; (B) vulnerability relationships using a scalar IM; (C) fragility models using a vector-valued IM; (D) vulnerability model using a vector-valued IM

deterioration models can well capture the stiffness and strength cyclic and in-cycle deterioration (using the E_H dissipated in each component), accentuated by the P-Δ effects. Similar behaviour is presented in different empirical damage models, such as the Park and Ang damage index.[78] Nevertheless, the impact of duration on these relationships cannot be inferred directly without performing a relevant comparative analysis against relationships derived using different ground-motion records with different durations (e.g., using separate sets of short- and long-duration ground motions; for further discussion, see Otárola, Gentile, et al.[14]). Figure 7C and D show the fragility and vulnerability models obtained using $avgSA$ and Ds_{5-95} in a vector-valued format. The fragility and vulnerability models explicitly account for the ground-motion duration since $avgSA$ and Ds_{5-95} can jointly describe part of the variability of the developed PSDMs. It can be noticed from the results that ground-motion duration mainly impacts the higher DSs (i.e., DS3 and DS4), while the lower DSs (i.e., DS1 and DS2) are slightly affected (i.e., the variability in the probability of exceeding a DS as a function of Ds_{5-95} only increase for higher DSs); confirming that DSs less severe than collapse are impacted by duration as shown in Otárola, Gentile, et al.[14] and Otárola, Sousa, et al.[15] As ground-motion duration increases, the probability of exceeding a DS for a given IM level increases (i.e., lower fragility median values are obtained); this explains why the vulnerability model exhibits a steady rise in the loss ratio due to duration. Since both the fragility and vulnerability models indicate an increasing trend in DS exceedance probability and LR, respectively, when $avgSA$ and Ds_{5-95} levels increase, it is inferred that duration can effectively impact the damage/loss estimates. In general, duration impact is more apparent at high $avgSA$ levels and conversely less significant at low $avgSA$ levels, providing a non-negligible impact on the nonlinear structural performance of the structures in analysis. Clearly, the fragility and vulnerability models are structure-dependent; therefore, these models vary accordingly for each case (not shown here for brevity). However, the presented results are consistent among all the building typologies considered in this study. It is worth mentioning that the fragility/vulnerability models conditioned on a scalar IM roughly represent a slice of those conditioned on a vector-valued IM around the median Ds_{5-95} value of the ground motions utilised. Hence, the vector-valued-based fragility/vulnerability models can provide higher or lower

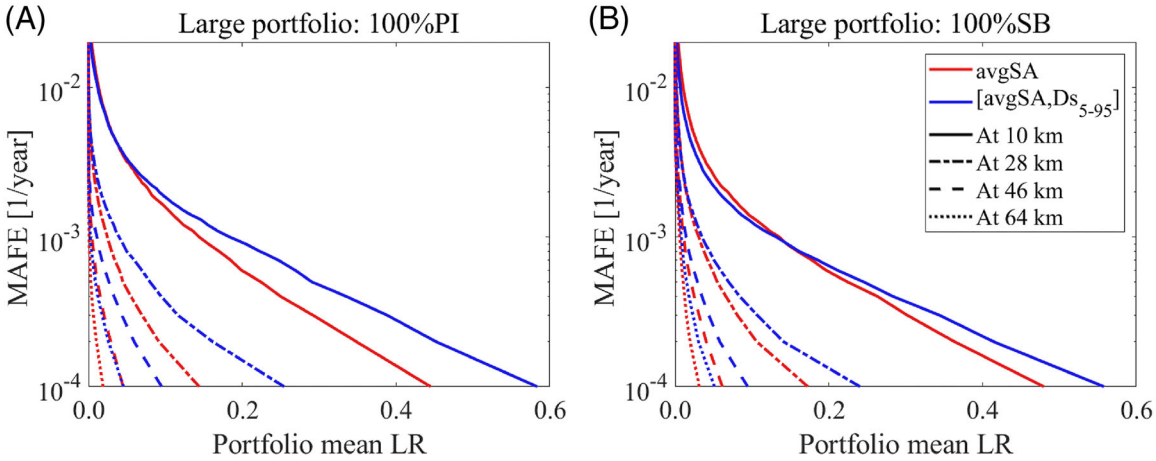

FIGURE 8 Median loss exceedance curves at distinct positions from the fault for a large portfolio composed by: (A) 100%PI; (B) 100%SB

probabilities of exceedance a DS/building mean LRs compared to the companion scalar-based ones. The last aspect is important when analysing the obtained portfolios' loss exceedance curves/EALs.

4.3 | Effects of ground-motion duration on losses

The simulated seismic losses are aggregated to derive portfolio-level estimates. The (median) loss exceedance curves of the large-size portfolios for the various exposure configurations are estimated at different distances from the fault, noting that the trends herein discussed are consistent when varying the portfolios' size. The 100%PI portfolio's (Figure 8A) loss exceedance curves derived using scalar and vector-valued IMs present considerable differences for MAFEs lower than 4×10^{-3} year^{-1}. Above this threshold, the differences are not significant. The reason behind it is that for low $avgSA$ and Ds_{5-95} levels, there exists good agreement between the developed models using the scalar and the vector-valued IMs; however, as the $avgSA$ level increase, the building mean LRs increase monotonically with the Ds_{5-95} level (i.e., the resulting vulnerability relationships as a function of Ds_{5-95} become steeper; see Figure 7D for an example of this tendency). The observed trend between the loss exceedance curves indicates that it is likely to obtain building mean LRs that increase suddenly at relatively short durations as the ground-motion amplitude increases; this result is directly propagated when aggregating the losses at the portfolio level. This is not the case of the 100%SB portfolio (Figure 8B), where significant differences in loss exceedance curves are noticed at MAFEs both lower and higher than 1×10^{-3} year^{-1}. Following the previous discussion, this indicates that it is likely to obtain building mean LRs that increase gradually within the duration range as the ground-motion amplitude increases; this result is propagated when aggregating the losses at the portfolio level in the same way. The 100%SI portfolio (not shown for brevity) exhibits qualitatively comparable results to the 100%PI one (behaviour that seems particular to the infilled frames), although showing a lower portfolio mean LRs due to the comparatively lower vulnerability of the buildings that make up this portfolio. Regarding the mixed portfolio (i.e., 60%PI + 32%SI + 8%SB; Figure 9A), the portfolio mean LRs attained are a direct propagation of the linear combination of the other portfolios' results. Since PI frames dominate the exposure in this mixed configuration, the overall trend is similar to that of the 100%PI portfolio, with slightly lower portfolio mean LRs given the other portfolios' contributions. It is also observed how the distance from the fault plays a fundamental role in the loss estimations, and the portfolio mean LRs decreases rapidly with increased distance in every case-study building portfolio. It seems that the mean LRs are higher near the source at 10 km (e.g., up to 0.5 for the large-mixed portfolio LRs conditioning on a vector-valued IM), but can decrease by more than half the previous results if the same portfolio is located at 28 km from the same fault. Another trend implies that as the portfolio-to-fault distance increases, the difference between the loss curves using the scalar and vector-valued IMs increases because duration impact is explicitly captured in the latter curves (i.e., since ground-motion duration increases with the distance from the fault). It is worth noting that scalar-based results are selected as a benchmark to compare against the – most-refined – vector-valued ones since the former are commonly derived in practice.

To better understand how the distance from the fault influences the loss estimates when accounting explicitly for duration, Figure 9A and B presents the relative variation between the (median) loss exceedance curves attained when using a

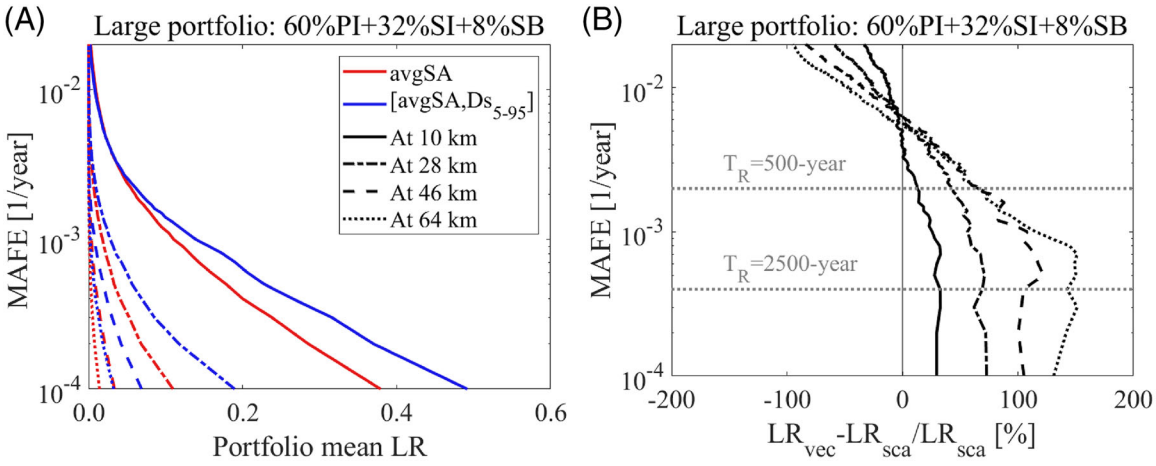

FIGURE 9 (A) Median loss exceedance curves at distinct positions from the fault for a large-mixed portfolio; (B) relative variation between the loss exceedance curves. Results obtained using a scalar IM are used as a benchmark case

scalar and a vector-valued IM. For example, for the large-mixed portfolio (Figure 9A), the scalar and vector-valued based loss curves intersect at approximately a MAFE of 4×10^{-3} year^{-1} since the buildings' vulnerability models conditioning on vector-valued IMs provides lower building's mean LRs for earthquake events producing minor $avgSA$ and Ds_{5-95} levels as mentioned above. It is worth noting that even though the relative variations are high above the said threshold, the differences are not significant for engineering purposes. Second, it is noticed that the relative variation of the portfolios' loss exceedance curves increases with the distance (Figure 9B), indicating that the further from the fault a portfolio is positioned, the more likely it is to obtain higher portfolio mean LRs by using buildings' vulnerability models conditioned on vector-valued IMs. The distance from the fault is measured as the distance from the source to the nearest portfolio's location (Figure 4A). When moving away from the fault, the amplitude-based IM (i.e., $avgSA$) decreases rapidly, but the duration-based IM (i.e., Ds_{5-95}) increases rapidly on the other hand, explaining the above-described relative variations. As noticed, these discrepancies are not present for building portfolios located beyond 40 km from the fault for earthquake events with T_R = 500-year (i.e., no significant building damage is found after 40 km). Nevertheless, the relative variations always increase for an earthquake event with T_R = 2500 year; but, seems to roughly stabilise after this value. Therefore, it is inferred that the duration impact can be particularly high when assessing the loss of building portfolios located relatively far from a fault (especially in the presence of soft soils as in this study) under a major ground shaking, up to a distance value such that the ground-motion amplitude is too low to cause any damage to the buildings within the considered portfolio.

Figure 10A–D depicts the calculated normalised EAL for eight of the assembled building portfolios, considering all the combinations of exposure configuration and the large and small sizes only. Figure 10A and B compares the building portfolios' EALs estimated for various distances from the fault. It is observable that the EAL decreases rapidly with distance as expected for the same reasons explained above for the portfolio mean LRs, where the ground-motion duration increases and the amplitude decreases with the distance from the fault; the highest significant differences occur between about 20 to 50 km as it is observed. Furthermore, it is apparent how the normalised EAL decreases with the increasing size of the portfolios since, according to their particular definition, larger portfolios have a higher number of locations affected by lower $avgSA$ levels. Moreover, due to the uniform composition of each portfolio location, the exposure configuration does not change the overall trends herein described. Figure 10C and D depicts the relative variation between the normalised EAL as the portfolio-to-fault distance increases. For every case except those located at distances below 20 km from the fault, the EAL tends to be significantly higher when using the vector-valued IM rather than the scalar one. The previous seems to follow a positive (i.e., increasing) trend, with relative variations up to about 200% for the farthest locations. This confirms that the further away a portfolio is positioned from the fault, higher portfolio normalised EALs are expected when using a vector-valued IM for the analysed site conditions. The portfolio size does not seem to affect the increasing trend depicted. Still, lower relative variations are found as the size decreases since the EAL values are found to be higher for smaller portfolios.

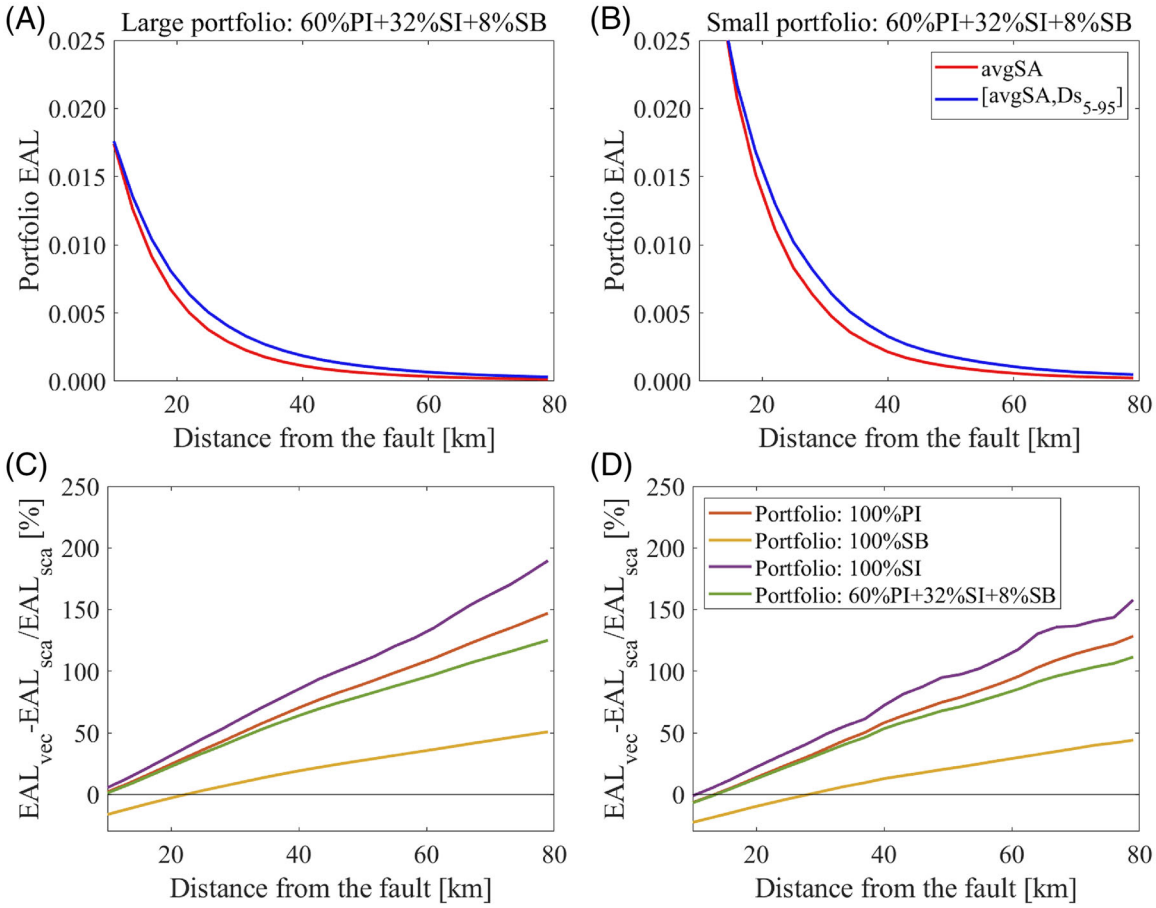

FIGURE 10 (A) EAL for large-mixed portfolio; (B) EAL for small-mixed portfolio; (C) relative variation for large-mixed portfolio; (D) relative variation for small-mixed portfolio. Results obtained using a scalar IM are used as a benchmark case

5 | CONCLUSIONS

This study investigated the influence of earthquake-induced ground-motion duration on estimating seismic losses for building portfolios using a simulation-based loss assessment framework. The aim was to examine how this ground-motion characteristic influences direct economic loss estimates, investigating whether duration matters (depending on the portfolio's size, position, and composition) and should be included in catastrophe (seismic) risk modelling. The proposed approach relied on event-based PSHA, cloud-based vulnerability derivation, and simulation-based loss estimation (i.e., explicitly accounting for duration in the seismic risk assessment framework's hazard, vulnerability and loss modules). In total, 12 building portfolios of different sizes and compositions (i.e., exposures) were used, located next to a case-study strike-slip fault and moved away from it to study how the loss estimations varied with the fault-to-portfolio distance. The portfolio sizes range from 81 to 1296 km^2, while the portfolios are composed – individually and in combination – of gravity-designed RC infilled building frames and seismically-designed RC infilled and bare frames. The main conclusions of this study are summarised as follows:

- It is verified that building-portfolio direct economic loss estimates are impacted by duration: its effects on these estimates depend on the portfolios' size, exposure composition, position from the fault, site conditions and the seismic source model describing a region's seismicity.
- The implemented simulation-based approach captures both the between- and within-event aleatory variability in the ground-motion fields efficiently;
- Fragility and vulnerability models conditioning on a vector-valued IM can better capture the impact of duration since E_H is utilised as EDP and Ds_{5-95} as one of the IMs. Therefore, damage accumulation is adequately described, given that E_H increases monotonically with the duration of the seismic excitation;

- The portfolio loss exceedance curves and EALs decrease rapidly as the fault-to-portfolio distance increases. This is due to the quick decline of the *avgSA* intensity with the distance from the fault. However, since duration increases with the same distance, the vector-valued vulnerability-based loss results are consistently higher than the scalar counterparts, particularly for higher return periods;
- The portfolio EAL increase as the size of the portfolios decreases since larger portfolios have a comparatively higher number of locations affected by lower *avgSA* levels. The relative variation (between using scalar- or vector-valued IMs) in the outcomes displays an increasing trend with the distance from the fault, regardless of the portfolio size or exposure composition.

Overall, ground-motion duration was found to provide a non-negligible impact on the direct economic losses for this particular study, observing an increasing influence of duration as the fault-to-portfolio distance increases. Therefore, it is concluded that the potential implications of duration should be investigated when performing a seismic risk assessment, especially in regions prone to long-duration ground motions (e.g., in the presence of soft soils) and/or portfolios with buildings (structures in general) prone to damage accumulation located relatively far from the source (i.e., from a distance where the ground-motion amplitude is not too high to overshadow the duration effects, up to a distance where it is too low to cause any damage to the portfolios' buildings). However, it is worth noting that the case-study results of this paper should not be generalised; instead, the proposed framework should be applied on a case-by-case basis to justify whether duration influences the loss estimates in a specific region. In fact, essential aspects such as the portfolio's size, exposure composition, and source models, among others, vary region by region. Additionally, the conclusions of this study depend on the adopted procedure to convert MIDR-based DS thresholds into E_H-based ones. Although the proposed approach is rational, experimental validation of the results is advisable.

ACKNOWLEDGEMENTS

This research has been developed within the framework of the project "Dipartimenti di Eccellenza", funded by the Italian Ministry of Education, University and Research at IUSS Pavia. Verisk – Extreme Event Solutions London office is gratefully acknowledged. Dr Roberto Gentile and Dr Carmine Galasso acknowledge funding from UKRI GCRF under grant NE/S009000/1, Tomorrow's Cities Hub. The authors also thank Prof Jack Baker (Stanford University) and an anonymous reviewer for their constructive feedback.

DATA AVAILABILITY STATEMENT

The data that support the findings of this study are available from the corresponding author upon reasonable request

ORCID

Kenneth Otárola https://orcid.org/0000-0002-5425-4423
Roberto Gentile https://orcid.org/0000-0002-7682-4490
Carmine Galasso https://orcid.org/0000-0001-5445-4911

REFERENCES

1. Silva V, Crowley H, Varum H, Pinho R. Seismic risk assessment for mainland Portugal. *Bull Earthquake Eng*. 2015;13(2):429-457. 10.1007/s10518-014-9630-0
2. Chandramohan R, Baker JW, Deierlein GG. Impact of hazard-consistent ground motion duration in structural collapse risk assessment. *Earthq Eng Struct Dyn*. 2016a;45(8):1357-1379. 10.1002/eqe.2711
3. Chaulagain H, Rodrigues H, Silva V, Spacone E, Varum H. Seismic risk assessment and hazard mapping in Nepal. *Natural Hazards*. 2015;78(1):583-602. 10.1007/s11069-015-1734-6
4. Bravo-Haro MA, Elghazouli AY. Influence of earthquake duration on the response of steel moment frames. *Soil Dyn Earthquake Eng*. 2018;115:634-651. 10.1016/j.soildyn.2018.08.027
5. Hwang SH, Mangalathu S, Jeon JS. Quantifying the effects of long-duration earthquake ground motions on the financial losses of steel moment resisting frame buildings of varying design risk category. *Earthq Eng Struct Dyn*. 2020;50:1451-1468. 10.1002/eqe.3403
6. Hancock J, Bommer JJ. A state-of-knowledge review of the influence of strong-motion duration on structural damage. *Earthquake Spectra*. 2006;22(3):827-845. 10.1193/1.2220576
7. Chandramohan R, Baker JW, Deierlein GG. Quantifying the influence of ground motion duration on structural collapse capacity using spectrally equivalent records. *Earthq Spectra*. 2016b;32(2):927-950. 10.1193/122813EQS298MR2
8. Cornell CA. Does Duration Really Matter? *FHWA/NCEER Workshop on the National Representation of Seismic Ground Motion for New and Existing Highway Facilities*. 1997:125-133.

9. Iervolino I, Manfredi G, Cosenza E. Ground motion duration effects on nonlinear seismic response. *Earthq Eng Struct Dyn*. 2006;35(1):21-38. 10.1002/eqe.529
10. Huang C, Tarbali K, Galasso C. Correlation properties of integral ground-motion intensity measures from Italian strong-motion records. *Earthq Eng Struct Dyn*. 2020;49(15):1581-1598. 10.1002/eqe.3318
11. Bradley BA. Correlation of significant duration with amplitude and cumulative intensity measures and its use in ground motion selection. *J Earthquake Eng*. 2011;15(6):809-832. 10.1080/13632469.2011.557140
12. Belejo A, Barbosa AR, Bento R. Influence of ground motion duration on damage index-based fragility assessment of a plan-asymmetric non-ductile reinforced concrete building. *Eng Struct*. 2017;151:682-703. 10.1016/j.engstruct.2017.08.042
13. Pan Y, Ventura CE, Tannert T. Damage index fragility assessment of low-rise light-frame wood buildings under long duration subduction earthquakes. *Struct Saf*. 2020;84:101940. 10.1016/j.strusafe.2020.101940
14. Otárola K, Gentile R, Sousa L, Galasso C. Impact of earthquake-induced ground-motion duration on nonlinear structural performance. Part I: spectrally equivalent records and inelastic single-degree-of-freedom systems. *Eartquake Spectra (under Review)*. 2022.
15. Otárola K, Sousa L, Gentile R, Galasso C. Impact of earthquake-induced ground-motion duration on nonlinear structural performance. Part II: site- and building-specific analysis. *Earthq Spectra (under Review)*. 2022.
16. Foschaar JC, Baker JW, Deierlein GG. Preliminary assessment of ground motion duration effects on structural collapse. 15th World Conference on Earthquake Engineering, 2011;22.
17. Bradley BA. A generalized conditional intensity measure approach and holistic ground-motion selection. *Earthq Eng Struct Dyn*. 2010;39(12). 10.1002/eqe.995
18. Du W, Yu X, Ning CL. Influence of earthquake duration on structural collapse assessment using hazard-consistent ground motions for shallow crustal earthquakes. *Bull Earthquake Eng*. 2020;18(7):3005-3023. 10.1007/s10518-020-00814-2
19. Jalayer F, Cornell CA. Alternative non-linear demand estimation methods for probability-based seismic assessments. *Earthq Eng Struct Dyn*. 2009;38(8):951-972. 10.1002/eqe.876
20. Baker JW. Probabilistic structural response assessment using vector-valued intensity measures. In: *Earthquake Engineering and Structural Dynamics*; 2007. 10.1002/eqe.700
21. Silva V, Crowley H, Pagani M, Monelli D, Pinho R. Development of the OpenQuake engine, the Global Earthquake Model's open-source software for seismic risk assessment. *Nat Hazards*. 2014;72(3):1409-1427. 10.1007/s11069-013-0618-x
22. Gentile R, Galasso C. Accounting for directivity-induced pulse-like ground motions in building portfolio loss assessment. *Bull Earthquake Eng*. 2020;19(15):6303-6328. 10.1007/s10518-020-00950-9
23. Mitchell-Wallace K, Jones M, Hillier J, Foote M. *Natural Catastrophe Risk Management and Modelling: A Practitioner's Guide*. Wiley-Blackwell; 2017.
24. Pagani M, Monelli D, Weatherill GA, Garcia J. *The OpenQuake-Engine Book*. GEM FOUNDATION; 2014.
25. Baker J, Bradley B, Stafford P. Seismic hazard and risk analysis. In: *Seismic Hazard and Risk Analysis*. 2021. 10.1017/9781108425056
26. Eads L, Miranda E, Lignos DG. Average spectral acceleration as an intensity measure for collapse risk assessment. *Earthq Eng Struct Dyn*. 2015;44(12):2057-2073. 10.1002/eqe.2575
27. Kohrangi M, Bazzurro P, Vamvatsikos D, Spillatura A. Conditional spectrum-based ground motion record selection using average spectral acceleration. *Earthq Eng Struct Dyn*. 2017;46(10):1667-1685. 10.1002/eqe.2876
28. Convertito V, Emolo A, Zollo A. Seismic-hazard assessment for a characteristic earthquake scenario: an integrated probabilistic-deterministic method. *Bull Seismol Soc Am*. 2006;96(2):377-391. 10.1785/0120050024
29. Wells DL, Coppersmith KJ. New empirical relationships among magnitude, rupture length, rupture width, rupture area, and surface displacement. *Bull Seismol Soc Am*. 1994;84(4):974-1002.
30. Joyner WB, Boore DM. Peak horizontal acceleration and velocity from strong-motion records including records from the 1979 imperial valley, California, earthquake. *Bull Seismol Soc Am*. 1981;71(6):2011-2038. 10.1785/bssa0710062011
31. Iacoletti S, Cremen G, Galasso C. Validation of the Epidemic-Type Aftershock Sequence (ETAS) models for simulation-based seismic hazard assessments. *Seismol Res Lett*. 2022;93:1601-1618.
32. Faure Walker JP, Visini F, Roberts G, Galasso C, McCaffrey K, Mildon Z. Variable fault geometry suggests detailed fault-slip-rate profiles and geometries are needed for fault-based probabilistic seismic hazard assessment (PSHA). *Bull Seismol Soc Am*. 2019;109(1):110-123. 10.1785/0120180137
33. Kazantzi AK, Vamvatsikos D. Intensity measure selection for vulnerability studies of building classes. *Earthq Eng Struct Dyn*. 2015;44(15):2677-2694. 10.1002/eqe.2603
34. Huang C, Galasso C. Ground-motion intensity measure correlations observed in Italian strong-motion records. *Earthq Eng Struct Dyn*. 2019;48(15):1634-1660. 10.1002/eqe.3216
35. Loth C, Baker JW. A spatial cross-correlation model of spectral accelerations at multiple periods. *Earthq Eng Struct Dyn*. 2013;42(3):397-417. 10.1002/eqe.2212
36. Jayaram N, Baker JW. Statistical tests of the joint distribution of spectral acceleration values. *Bull Seismol Soc Am*. 2008;98(5):2231-2243. 10.1785/0120070208
37. Iervolino I, Giorgio M, Galasso C, Manfredi G. Conditional hazard maps for secondary intensity measures. *Bull Seismol Soc Am*. 2010;100(6):3312-3319. 10.1785/0120090383
38. Markhvida M, Ceferino L, Baker JW. Modeling spatially correlated spectral accelerations at multiple periods using principal component analysis and geostatistics. *Earthq Eng Struct Dyn*. 2018;47(5):1107-1123. 10.1002/eqe.3007

39. Du W, Ning CL. Modeling spatial cross-correlation of multiple ground motion intensity measures (SAs, PGA, PGV, Ia, CAV, and significant durations) based on principal component and geostatistical analyses. *Earthq Spectra*. 2021;37(1):486-504. 10.1177/8755293020952442
40. Goda K, Hong HP. Spatial correlation of peak ground motions and response spectra. *Bull Seismol Soc Am*. 2008;98(1):354-365. 10.1785/0120070078
41. Bradley BA. A ground motion selection algorithm based on the generalized conditional intensity measure approach. *Soil Dyn Earthquake Eng*. 2012;40:48-61. 10.1016/j.soildyn.2012.04.007
42. Baker JW, Cornell CA. A vector-valued ground motion intensity measure consisting of spectral acceleration and epsilon. *Earthq Eng Struct Dyn*. 2005;34(10):1193-1217. 10.1002/eqe.474
43. Ibarra LF, Medina RA, Krawinkler H. Hysteretic models that incorporate strength and stiffness deterioration. *Earthq Eng Struct Dyn*. 2005;34(12):1489-1511. 10.1002/eqe.495
44. Lignos DG, Krawinkler H. Deterioration modeling of steel components in support of collapse prediction of steel moment frames under earthquake loading. *J Struct Eng*. 2011;137(11):1291-1302. 10.1061/(asce)st.1943-541x.0000376
45. Rahnama M, Krawinkler H. Effects of soft soil and hysteresis model on seismic demands. *John A Blume Earthq Eng Center Tech Rep Series*. 1993;TR108(108).
46. Belsley DA. A guide to using the collinearity diagnostics. *Comput Sci Econ Manag*. 1991;4(1):33-50. 10.1007/BF00426854
47. Gentile R, Galasso C. Hysteretic energy-based state-dependent fragility for ground-motion sequences. *Earthq Eng Struct Dyn*. 2021;50(4):1187-1203. 10.1002/eqe.3387
48. Quinde P, Terán-Gilmore A, Reinoso E. Cumulative structural damage due to low cycle fatigue: an energy-based approximation. *J Earthquake Eng*. 2021;25(12):2474-2494. 10.1080/13632469.2019.1692736
49. Terán Gilmore A. CONSIDERACIONES DE USO DE LA ENERGÍA PLÁSTICA EN EL DISEÑO SÍSMICO. *Revista de Ingeniería Sísmica*. 2001;65:81. 10.18867/ris.65.190
50. Erberik A, Sucuoğlu H. Seismic energy dissipation in deteriorating systems through low-cycle fatigue. *Earthq Eng Struct Dyn*. 2004;33(1):49-67. 10.1002/eqe.337
51. Scribner CF, Wight JK. STRENGTH DECAY IN R. C. BEAMS UNDER LOAD REVERSALS. *ASCE J Struct Div*. 1980;106(4):861-876. 10.1061/jsdeag.0005402
52. Bojórquez E, Iervolino I, Reyes-Salazar A, Ruiz SE. Comparing vector-valued intensity measures for fragility analysis of steel frames in the case of narrow-band ground motions. *Eng Struct*. 2012;45:472-480. 10.1016/j.engstruct.2012.07.002
53. Aljawhari K, Gentile R, Freddi F, Galasso C. Effects of ground-motion sequences on fragility and vulnerability of case-study reinforced concrete frames. *Bull Earthquake Eng*. 2020;19:6329-6359. 10.1007/s10518-020-01006-8
54. Di Pasquale G, Orsini G, Romeo RW. New developments in seismic risk assessment in Italy. *Bull Earthquake Eng*. 2005;3(1):101-128. 10.1007/s10518-005-0202-1
55. Dolce M, Kappos A, Masi A, Penelis G, Vona M. Vulnerability assessment and earthquake damage scenarios of the building stock of Potenza (Southern Italy) using Italian and Greek methodologies. *Eng Struct*. 2006;28(3):357-371. 10.1016/j.engstruct.2005.08.009
56. Kappos AJ, Panagopoulos G, Panagiotopoulos C, Penelis G. A hybrid method for the vulnerability assessment of R/C and URM buildings. *Bull Earthquake Eng*. 2006;4(4):391-413. 10.1007/s10518-006-9023-0
57. Silva V. Uncertainty and correlation in seismic vulnerability functions of building classes. *Earthq Spectra*. 2019;35(4):1515-1539. 10.1193/013018EQS031M
58. Minas S, Galasso C. Accounting for spectral shape in simplified fragility analysis of case-study reinforced concrete frames. *Soil Dyn Earthquake Eng*. 2019;119:91-103. 10.1016/j.soildyn.2018.12.025
59. Eurocode 8. *European Standard EN 1998-3:2005: Design of Structures for Earthquake Resistance – Part 3: Assessment and Retrofitting of Buildings*. Comite Europeen de Normalisation, 2005;3.
60. Consiglio dei ministri. Regio Decreto Legge n. 2229 del 16/11/1939. G.U. n.92 del 18/04/1940. 1939
61. Liberatore L, Mollaioli F. Influence of masonry infill modelling on the seismic response of reinforced concrete frames. *Civil-Comp Proceedings*. 2015. 10.4203/ccp.108.87
62. Mohammad Noh N, Liberatore L, Mollaioli F, Tesfamariam S. Modelling of masonry infilled RC frames subjected to cyclic loads: state of the art review and modelling with OpenSees. *Eng Struct*. 2017;150:599-621. 10.1016/j.engstruct.2017.07.002
63. Hak S, Morandi P, Magenes G. Local effects in the seismic design of RC frame structures with masonry infills. ECCOMAS Thematic Conference - COMPDYN 2013: 4th International Conference on Computational Methods in Structural Dynamics and Earthquake Engineering, Proceedings - An IACM Special Interest Conference. 2013. 10.7712/120113.4713.c1270
64. Haselton C. Assessing Seismic Collapse Safety of Modern Reinforced Concrete Moment Frame Buildings. *Stanford (CA): Department of Civil and Environmental Engineering*. Stanford University, Ph.D. Thesis. 2007.
65. Kohrangi M, Vamvatsikos D, Bazzurro P. Site dependence and record selection schemes for building fragility and regional loss assessment. *Earthq Eng Struct Dyn*. 2017;46(10):1625-1643. 10.1002/eqe.2873
66. Zhong K, Chandramohan R, Baker JW, Deierlein GG. Site-specific adjustment framework for incremental dynamic analysis (SAF-IDA). *Earthq Spectra*. 2022;38(3):1893-1917. 10.1177/87552930221083688
67. Forte G, Chioccarelli E, De Falco M, Cito P, Santo A, Iervolino I. Seismic soil classification of Italy based on surface geology and shear-wave velocity measurements. *Soil Dyn Earthquake Eng*. 2019;122:79-93. 10.1016/j.soildyn.2019.04.002
68. Luco N, Bazzurro P. Does amplitude scaling of ground motion records result in biased nonlinear structural drift responses? *Earthq Eng Struct Dyn*. 2007;36(13):1813-1835. 10.1002/eqe.695
69. Ancheta TD, Darragh RB, Stewart JP, et al. NGA-West2 Database. *Earthq Spectra*. 2014;30(3):989-1005. 10.1193/070913EQS197M

70. Barani S, Spallarossa D, Bazzurro P. Disaggregation of probabilistic ground-motion Hazard in Italy. *Bull Seismol Soc Am*. 2009;99(5):2638-2661. 10.1785/0120080348
71. Silva V. Critical issues on probabilistic earthquake loss assessment. *J Earthquake Eng*. 2018;22(9):1683-1709. 10.1080/13632469.2017.1297264
72. Boore DM, Thompson EM. Path durations for use in the stochastic-method simulation of ground motions. *Bull Seismol Soc Am*. 2014;104(5):2541-2552. 10.1785/0120140058
73. Stein S, Wysession M. *An Introduction to Seismology, Earthquakes, and Earth Structure*. Blackwell Publishing Ltd; 2003.
74. Trifunac MD, Brady AG. A study on the duration of strong earthquake ground motion. *Bull Seismol Soc Am*. 1978;65(3):581-626.
75. Dobry R, Idriss IM, Ng E. Duration characteristics of horizontal components of strong-motion earthquake records. *Bull Seismol Soc Am*. 1978;68(5):1487-1520.
76. Henze N, Zirkler B. A class of invariant consistent tests for multivariate normality. *Commun Stat Theory Methods*. 1990;19(10):3595-3617. 10.1080/03610929008830400
77. Baker JW, Bradley BA. Intensity measure correlations observed in the NGA-West2 database, and dependence of correlations on rupture and site parameters. *Earthq Spectra*. 2017;33(1):145-156. 10.1193/060716EQS095M
78. Park Y, Ang AH-S. Mechanistic seismic damage model for reinforced concrete. *J Struct Eng*. 1985;111(4):722-739. 10.1061/(asce)0733-9445(1985)111:4(722)
79. Burton H, Deierlein G. Simulation of seismic collapse in nonductile reinforced concrete frame buildings with masonry infills. *J Struct Eng*. 2014;140(8):A4014016. 10.1061/(asce)st.1943-541x.0000921
80. Haselton CB, Liel AB, Taylor-Lange SC, Deierlein GG. Calibration of model to simulate response of reinforced concrete beam-columns to collapse. *ACI Struct J*. 2016;113(6). 10.14359/51689245
81. Liberatore L, Decanini LD. Effect of infills on the seismic response of high-rise RC buildings designed as bare according to Eurocode 8 [Infl uenza della tamponatura sulla risposta sismica di edifi ci in c.a. alti progettati come nudi con l'Eurocodice 8]. *Ingegneria Sismica*. 2011;28(3):7-23.
82. Mazzoni S, McKenna F, Scott M, Fenves GL. Open system for earthquake engineering simulation user command-language manual, OpenSees version 2.0. University of California, Berkeley. 2009.
83. Panagiotakos TB, Fardis MN. Deformations of reinforced concrete members at yielding and ultimate. *ACI Struct J*. 2001;98(2). 10.14359/10181
84. Setzler EJ, Sezena H. Model for the lateral behavior of reinforced concrete columns including shear deformations. *Earthq Spectra*. 2008;24(2):493-511. 10.1193/1.2932078
85. Sezen H, Moehle JP. Shear strength model for lightly reinforced concrete columns. *J Struct Eng*. 2004;130(11):1692-1703. 10.1061/(asce)0733-9445(2004)130:11(1692)
86. Verderame GM, Ricci P, Esposito M, Sansiviero FC. Le caratteristiche meccaniche degli acciai impiegati nelle strutture in c.a. realizzate dal 1950 AL 1980 (in Italian). In: *Associazione Italiana Calcestruzzo Armato e Precompresso (AICAP)*. 2011.
87. Zareian F, Medina RA. A practical method for proper modeling of structural damping in inelastic plane structural systems. *Comput Struct*. 2010;88(1–2):45-53. 10.1016/j.compstruc.2009.08.001

How to cite this article: Otárola K, Gentile R, Sousa L, Galasso C. Accounting for earthquake-induced ground-motion duration in building-portfolio loss assessment. *Earthquake Engng Struct Dyn*. 2022;1-23. https://doi.org/10.1002/eqe.3791

APPENDIX A: NUMERICAL MODELLING STRATEGY

The frame computational models are developed by adopting the OpenSees v3.2.2 software.[82] The gravity loads are uniformly distributed on the beams, and the masses are concentrated at each floor master node. Elastic damping is modelled through the Rayleigh model,[86] using a 5.00% viscous damping ratio on the first two vibration modes. Geometric nonlinearities are included to account for the destabilising $P-\Delta$ effects. Beam-column end-offsets and floor diaphragms are both modelled as rigid components. A lumped plasticity approach is used for all the case-study frames to model both beams and columns' nonlinear behaviour using zero-length rotational springs. The Ibarra-Medina-Krawinkler[43,44] model with peak-oriented hysteretic response is implemented to define the moment-rotation relationship of the rotational springs (including stiffness and strength cyclic and in-cycle deterioration). The yielding bending moment and yielding rotation are determined according to Panagiotakos and Fardis,[83] while the other parameters (i.e., initial stiffness, hardening stiffness, maximum bending moment, rotation at the onset of capping, softening stiffness, post-capping rotation) are defined according to Haselton et al.[80] For the PI frame, nonlinear shear springs are added in series to the rotational ones to account for potential shear failures through the Hysteretic material in OpenSees. The Setzler and Sezen[84] model is implemented to define the force-deformation relationship of the shear springs. It is characterised by the maximum shear strength (calculated according to Sezen and Moehle[85]), shear deformation at the onset of peak shear strength, the shear deformation

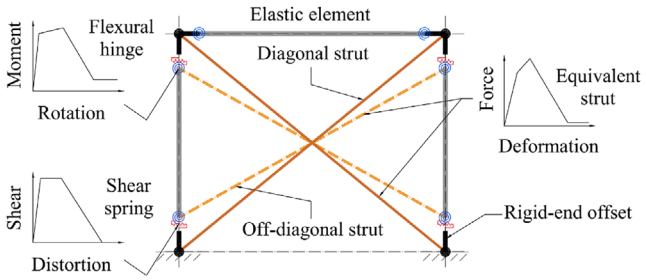

FIGURE A1 Scheme of the numerical modelling strategy for beams, columns, and masonry infills (including backbones). Shear springs and equivalent diagonal and off-diagonal struts do not apply to the SB frame. Shear springs and equivalent off-diagonal struts do not apply to the SI frame

at the beginning of shear failure, and the shear deformation at the axial load failure. It is worth highlighting that, for simplicity, shear springs are disregarded in the special-code frames, which exhibit a global beam-sway mechanism. In fact, the shear failure mode is unlikely to develop in such frames due to modern seismic design provisions. Masonry infill walls are modelled as equivalent diagonal struts connecting beam-column intersections to account for their effect on the global response of the case-study frames. The force-deformation relationship (implemented through the Hysteretic material in OpenSees) introduced by Liberatore and Decanini[81] is assigned to the equivalent struts characterising the behaviour of infills, which accounts for four possible failure modes: diagonal tension, sliding shear, corner crushing and diagonal compression. The parameters describing the hysteretic response of infills are adopted from Mohammad Noh et al.[62] Diagonal struts which connect the nodes at the beam-column intersections are used to model the masonry infills for the SI frame, infills are modelled using Burton and Deierleins'[79] double strut approach for the PI frame. In such a case, one diagonal strut connecting the beam-column joints and another off-diagonal strut connecting the column shear springs are modelled. According to Burton and Deierlein,[79] 75% of the total infill strength and stiffness is assigned to the diagonal strut, while 25% is assigned to the off-diagonal one. Such a modelling strategy does not simulate the entire distribution of column shear due to the frame-infill interaction. Still, it captures the increase of shear demands in columns, thus allowing possible changes in the overall plastic mechanism of the frame. A complete description of the employed models and additional details can be found in Aljawhari et al.[53] Figure A1 shows a scheme of the adopted nonlinear modelling strategy (specifically for an example frame with a single storey and a single bay).